WRF-Chem simulated surface ozone over South Asia during the pre-monsoon: Effects of emission inventories and chemical mechanisms

Amit Sharma[1, 2, *], Narendra Ojha[2, *], Andrea Pozzer[2], Kathleen A. Mar[3], Gufran Beig[4], Jos Lelieveld[2, 5], and Sachin S. Gunthe[1]

[1]Department of Civil Engineering, Indian Institute of Technology Madras, Chennai, India
[2]Atmospheric Chemistry Department, Max Planck Institute for Chemistry, Mainz, Germany
[3]Institute for Advanced Sustainability Studies, Potsdam, Germany
[4]Indian Institute for Tropical Meteorology, Pune, India
[5]Energy, Environment and Water Research Center, The Cyprus Institute, Nicosia, Cyprus

[*]*Correspondence to*: Amit Sharma (amit.iit87@gmail.com) and Narendra Ojha (narendra.ojha@mpic.de)

Abstract

We evaluate numerical simulations of surface ozone mixing ratios over the South Asian region during the pre-monsoon season, employing three different emission inventories (EDGAR-HTAP, INTEX-B, and SEAC4RS) in the WRF-Chem model with the RADM2 chemical mechanism. Evaluation of modelled ozone and its diurnal variability, using data from a network of 18 monitoring stations across South Asia, shows the model ability to reproduce the clean, rural and polluted urban conditions over this region. In contrast to the diurnal average, the modelled ozone mixing ratios during noontime i.e. hours of intense photochemistry (1130-1630 h Indian Standard Time or IST) are found to differ among the three inventories. This suggests that evaluations of the modelled ozone limited to 24-h average are insufficient to assess uncertainties associated with ozone build-up. HTAP generally shows 10-30 ppbv higher noontime ozone mixing ratios than SEAC4RS and INTEX-B, especially over the north-west Indo-Gangetic Plain (IGP), central India and southern India. Further, the model performance shows strong spatial heterogeneity, with SEAC4RS leading to better agreement with observations over east and south India, whereas HTAP performs better over north and central India, and INTEX-B over west India. The Normalized Mean Bias (NMB in %) in the noontime ozone over the entire South Asia is found to be lowest for the SEAC4RS (~11%), followed by INTEX-B (~12.5%) and HTAP (~22%). The HTAP simulation repeated with the alternative MOZART chemical mechanism showed even more strongly enhanced surface ozone mixing ratios (noontime NMB=36.5%) due to vertical mixing of enhanced ozone that has been produced aloft. The SEAC4RS inventory with the RADM2 chemical mechanism is found to be the most successful overall among the configurations evaluated here in simulating ozone air quality over South Asia. Our study indicates the need to also evaluate the O_3 precursors across a network of stations to further reduce uncertainties in modelled ozone. We also recommend preparing high-resolution regional inventories for the anthropogenic emissions of O_3 precursors over South Asia that also account for year-to-year changes.

1. Introduction

Tropospheric ozone plays central roles in atmospheric chemistry, air quality and climate change. Unlike primary pollutants, which are emitted directly, tropospheric ozone forms photochemically involving precursors such as carbon monoxide (CO), volatile organic compounds (VOCs) and oxides of nitrogen (NO_x), supplemented by transport from the stratosphere (e.g. Crutzen, 1974; Atkinson, 2000; Monks et al., 2015). It can be transported over long distances resulting in enhanced concentrations even in areas located remote from the sources of precursors (Cox et al., 1975). The photochemical production of ozone and its impacts on agricultural crops and human health are especially pronounced near the surface. Numerous studies have shown that elevated surface ozone levels significantly reduce crop yields (e. g.; Krupa et al., 1998; Emberson et al., 2009; Ainsworth et al., 2012; Wilkinson et al., 2012), in addition to adverse human health effects that cause premature mortality (e.g., Bell et al., 2004; Jerrett et al., 2009; Anenberg et. al., 2010; Lelieveld et al., 2015).

An accurate representation of anthropogenic emissions of ozone precursors is essential to understand the photochemical production of ozone and support policy making. While anthropogenic emissions have been nearly stable or decreasing over northern America and Europe (e. g. Yoon and Pozzer, 2014), there has been substantial enhancement over the East and South Asian regions in recent decades (e. g. Akimoto, 2003; Ohara et al., 2007, Logan et al., 2012; Gurjar et al., 2016). The number of premature mortalities per year due to outdoor air pollution is anticipated to double by the year 2050 as compared to the year 2010 in a business-as-usual scenario, predominantly in Asia (Lelieveld et al., 2015). The multi-pollutant index over all populated regions in the northern hemisphere shows a general increase, with South Asia being the major hotspot of deteriorating air quality (Pozzer et al., 2012).

The growth of anthropogenic emissions over the South Asian region has regional implications, and is also predicted to influence air quality on a hemispheric scale (Lelieveld and Dentener, 2000). It was shown that the anthropogenic emissions and their subsequent photochemical degradation over South Asia influence air quality over the Himalayas (e.g. Ojha et al., 2012; Sarangi et al., 2014) and the Tibetan Plateau (Lüthi et al., 2015) as well as the marine environment downwind of India (e.g. Lawrence and Lelieveld, 2010). Additionally, the prevailing synoptic scale weather patterns make this region highly conducive to long-range export of pollutants (e.g. Lelieveld et al., 2002; Lawrence et al., 2003; Ojha et al., 2014; Zanis et al., 2014). Therefore, the accurate estimation of anthropogenic emissions over South Asia and their representation in chemical transport models are essential to quantify the effects on regional as well as global air quality.

The Weather Research and Forecasting model with Chemistry (WRF-Chem) (Grell et al., 2005; Fast et al., 2006), a regional simulation system, has been popular for use over the South Asian region in numerous recent studies to simulate the meteorology and spatio-temporal distribution of ozone and related trace gases (e. g. Kumar et al., 2012a, 2012b; Michael et al., 2013; Gupta et al., 2015; Jena et al., 2015; Ansari et al., 2016; Ojha et al., 2016; Girach et al., 2017). WRF-Chem simulations at higher spatial resolution employing regional emission inventories have been shown to better reproduce the observed spatial and temporal heterogeneities in ozone over this region as compared to the global models (e.g. Kumar et al., 2012b; Ojha et al., 2016). However, an evaluation of modelled ozone based on data from a network of stations across South Asia is imperative considering very large spatio-temporal heterogeneity in the distribution of ozone over this region (e.g. Kumar et al., 2010; Ojha et al., 2012; Kumar et al., 2012b) mainly resulting from heterogeneous precursor sources and population distribution. WRF-

Chem simulated ozone distributions have also been utilized to assess the losses in crop yields, and it was suggested that the estimated crop losses would be sufficient to feed about 94 million people living below the poverty line in this region (Ghude et al., 2014). Further, WRF-Chem has been used to estimate that premature mortality in India caused by chronic obstructive pulmonary disease (COPD) due to surface O_3 exposure was ~12,000 people in the year 2011 (Ghude et al., 2016). Despite these applications, there is room for improvement in modeled concentrations as some limited studies evaluating ozone on diurnal scales revealed a significant overestimation of noontime ozone e.g. by as much as 20 ppbv in Kanpur (Michael et al., 2013) and 30 ppbv in Delhi (Gupta and Mohan, 2015).

Using WRF-Chem, Amnuaylojaroen et al. (2014) showed that over continental southeast Asia surface ozone mixing ratios vary little (~4.5%) among simulations employing different emission inventories. A recent study by Mar et al. (2016) highlighted the dependence of WRF-Chem predicted ozone air quality (over Europe) on the chosen chemical mechanism. These results indicate the need for evaluating the effects of emission inventories and chemical mechanisms on the model performance using a network of stations across South Asia, which has not been carried out thus far. The main objectives of the present study are:

(a) To evaluate WRF-Chem simulated ozone over South Asia, including the diurnal cycle, against recent in situ measurements from a network of stations;
(b) To inter-compare model simulated O_3 among different emission inventories;
(c) To inter-compare model simulated O_3 between two extensively used chemical mechanisms (MOZART and RADM2) with the same emission inventory;
(d) To provide recommendations on the model configuration for future studies over stations, sub-regions as well as the entire South Asian region.

We focus on the pre-monsoon season (March-May) for the study as O_3 mixing ratios at the surface are generally the highest over most of South Asia during this period (Jain et al., 2005; Debaje et al., 2006; Reddy et al., 2010; Ojha et al., 2012; Gaur et al., 2014; Renuka et al., 2014; Bhuyan et al., 2014; Sarangi et al., 2014; Yadav et al., 2014; Sarkar et al., 2015). This is because photochemistry over South Asia is most intense during this season caused by the combined effects of high pollution loading, biomass-burning emissions and a lack of precipitation. The effects of biomass burning on ozone in Southern Asia have been studied by Jena et al. (2014) reporting O_3 enhancements of 4-10 ppb (25-50%) in the Eastern region including Burma, 1-3 ppb (10-25%) in Central India and 1-7 ppb (4-10%) in the Indo-Gangetic region. Further, the O_3 enhancement was found to be about 2-6 ppb (8-20%) over the Bay of Bengal in March, which was attributed to transport from the Eastern region. Section 2 presents the model description, including physics and chemistry options, emission inputs and the observational data. Model evaluation focussing on the effects of different emission inventories on ozone is presented in section 3. The inter-comparison between the RADM2 and MOZART chemical mechanism is discussed in section 4. The sub-regional and South Asian domain evaluation and recommendations on model configuration are provided in section 5, followed by the summary and conclusions drawn from the study in section 6. The list of abbreviations and acronyms used in this paper are listed in Table 1.

2. Methodology

2.1. WRF-Chem

In this study we use the Weather Research and Forecasting model coupled with chemistry (WRF-Chem version 3.5.1), which is an online mesoscale model capable of simulating meteorological and chemical processes simultaneously (Grell et al., 2005; Fast et al., 2006). The model domain (Fig. 1) is defined on a mercator projection and is centred at 22^0 N, 83^0 E with 274 and 352 grid points in the east-west and north-south directions, respectively, at the horizontal resolution of 12 km x 12 km. The land use data is incorporated from the US Geological Survey (USGS) based on 24 land use categories. The ERA-interim reanalysis dataset from ECMWF (http://www.ecmwf.int/en/research/climate-reanalysis/browse-reanalysis-datasets), archived at the horizontal resolution of about 0.7^o and temporal resolution of 6 hours, is used to provide the initial and lateral boundary conditions for the meteorological calculations. All simulations in the study have been conducted for the period: 26^{th} February – 31^{st} May, 2013 at a time step of 72 s. The model output is stored every hour for analysis. The first three days of model output have been discarded as model spin up.

Radiative transfer in the model has been represented using the Rapid Radiative Transfer Model (RRTM) longwave scheme (Mlawer, 1997) and the Goddard shortwave scheme (Chou and Suarez, 1994). Surface physics is parameterized using the Unified Noah land surface model (Tewari et al., 2004) along with eta similarity option (Monin and Obukhov, 1954; Janjic, 1994, 1996), and the planetary boundary layer (PBL) is based on the Mellor-Yamada-Janjic (MYJ) scheme (Mellor and Yamada, 1982; Janjic, 2002). The cloud microphysics is represented by the Lin et al. scheme (Lin et. al., 1983), and cumulus convection is parameterized using the Grell 3D Ensemble Scheme (Grell, 1993; Grell and Devenyi, 2002). Four-dimensional data assimilation (FDDA) is incorporated for nudging to limit the drift in the model simulated meteorology from the ERA-interim reanalysis (Stauffer and Seaman, 1990; Liu et al. 2008). Horizontal winds are nudged at all vertical levels, whereas temperature and water vapour mixing ratios are nudged above the PBL (Stauffer et al. 1990, 1991). The nudging coefficients for temperature and horizontal winds are set as 3×10^{-4} s^{-1} whereas it is set as 10^{-5} s^{-1} for water vapour mixing ratio (Otte, 2008).

This study utilizes two different chemical mechanisms, the Regional Acid Deposition Model - 2^{nd} generation (RADM2) (Stockwell et al., 1990), and the Model for Ozone and Related Chemical Tracers-version 4 (MOZART-4) (Emmons et al., 2010). RADM2 chemistry includes 63 chemical species participating in 136 gas phase and 21 photolysis reactions. MOZART chemistry includes 81 chemical species participating in 159 gas phase and 38 photolysis reactions. Aerosols are represented using the Modal Aerosol Dynamics Model for Europe/ Secondary Organic Aerosol Model (MADE/ SORGAM) (Ackermann et al., 1998; Schell et al., 2001) with RADM2 and Global Ozone Chemistry Aerosol Radiation and Transport (GOCART) (Chin et al., 2000) with MOZART. The photolysis rates are calculated using the Fast-J photolysis scheme (Wild et al., 2000) in RADM2 simulations and the Madronich FTUV scheme in the MOZART simulation. In WRF-Chem, the Madronich F-TUV photolysis scheme uses climatological O_3 and O_2 overhead columns. The treatment of dry deposition process also differs between RADM2 and MOZART owing to differences in Henry's Law coefficients and diffusion coefficients. The chemical initial and lateral boundary conditions are provided from 6 hourly fields from the Model for Ozone and Related Chemical Tracers (MOZART-4/GEOS5) (http://www.acom.ucar.edu/wrf-chem/mozart.shtml).

158 **2.2. Emission inputs**

159 This study utilizes three different inventories for the anthropogenic emissions: HTAP, INTEX-B and the
160 SEAC4RS, which are briefly described here. The Hemispheric Transport of Air Pollution (HTAP) inventory
161 (Janssens-Maenhout et al., 2015) for anthropogenic emissions (http://edgar.jrc.ec.europa.eu/htap_v2
162 /index.php?SECURE=_123) available for the year 2010 has been used. The HTAP inventory has been developed
163 by complementing various regional emissions with EDGAR data, in which Asian region including India is
164 represented by the Model Intercomparison study for Asia (MICS-Asia) inventory, which is at a horizontal
165 resolution of 0.25^o x 0.25^o (Carmichael et al., 2008). The resultant global inventory is re-gridded at the spatial
166 resolution of 0.1^o x 0.1^o and temporal resolution of 1 month. HTAP includes emissions of CO, NO_x, SO_2,
167 NMVOCs, PM, BC and OC from power, industry, residential, agriculture, ground transport and shipping sectors.
168 The Intercontinental Chemical Transport Experiment-Phase B (INTEX-B) inventory (Zhang et al., 2009),
169 developed to support the INTEX-B field campaign by the National Aeronautics and Space Administration
170 (NASA) in spring 2006, is the second inventory used in this study. It provides total emissions for year 2006 at a
171 horizontal resolution of 0.5^o x 0.5^o. The emission sectors include power generation, industry, residential and
172 transportation. The Southeast Asia Composition, Cloud, Climate Coupling Regional Study (SEAC4RS) inventory
173 (Lu and Streets, 2012), prepared for the NASA SEAC4RS field campaign, is the third inventory used in this study.
174 It provides total emissions for the year 2012 at a spatial resolution of 0.1^o x 0.1^o. The SEAC4RS and INTEX-B did
175 not cover regions in the north western part of the domain, and therefore we complemented this region (longitude <
176 75^oE and latitude > 25^oN) by HTAP emission data. The emissions of CO, NMVOCs and NO_x emissions among
177 the three emission inventories, as included in the simulations, are shown in Fig. 2. Table 2 provides estimates of
178 total emissions over different regions (as defined in Fig.1) from the three inventories. The total emissions over all
179 regions show that HTAP has about 43% higher and SEAC4RS about 46% higher NO_x emissions compared to the
180 INTEX-B inventory. Also, HTAP has about 37% higher VOC emissions compared to SEAC4RS and about 49%
181 higher compared to the INTEX-B inventory. Hence SEAC4RS, the most recent inventory of the three, has similar
182 total NO_x emissions as that in HTAP but the total VOC source is closer to INTEX-B, which is the oldest of the
183 three inventories. Considering the non-linear dependence of O_3 formation on precursors, numerical experiments
184 are necessary to assess the influence of such large differences among the inventories. The emissions from biomass
185 burning are included using the Fire Inventory from NCAR (FINN) version 1.0 (Wiedinmyer et al., 2011). Model
186 of Emissions of Gases and Aerosols from Nature (MEGAN) is used to include the biogenic emissions (Guenther et
187 al., 2006) in the model.

188 The HTAP inventory is available at monthly temporal resolution while INTEX-B and SEAC4RS are available as
189 annual averages; however, seasonal variability in anthropogenic emissions may not have a major effect in this
190 study as we focus here on spring (pre-monsoon), for which monthly emissions are similar to the annual mean
191 (seasonal factor close to unity) (Supplementary material - Fig. S1; also see Fig. 2b in Kumar et al., 2012b).
192 Nevertheless, seasonal influence during spring is strongest for biomass-burning emissions, which have been
193 accounted for. The emissions from all inventories were injected in the lowest model layer. The diurnal profiles of
194 the anthropogenic emissions of ozone precursors, specific to South Asia are not available. A sensitivity simulation
195 implementing the diurnal emission profile available for Europe (Mar et al., 2016 and references therein) showed a
196 little impact on predicted noontime ozone over South Asia (Supplementary material – Fig S2).

197

198 **2.3. Simulations**

199 We have conducted 4 different numerical simulations as summarized in Table 3 and briefly described here. Three
200 simulations correspond to three different emission inventories HTAP, INTEX-B and SEAC4RS for the
201 anthropogenic emissions of ozone precursors, employing the RADM2 chemical mechanism. These simulations are
202 named HTAP-RADM2, INTEX-RADM2 and S4RS-RADM2 respectively. The emissions of aerosols have been
203 kept same (HTAP) among these three simulations and aerosol-radiation feedback has been switched off to
204 specifically identify the effects of emissions of O_3 precursors on modelled ozone. An additional simulation HTAP-
205 MOZ has been conducted to investigate the sensitivity of ozone to the employed chemical mechanism (MOZART
206 vs RADM2) by keeping the emissions fixed to HTAP.

207 **2.4. Observational dataset**

208 Previous studies have shown that WRF-Chem accurately reproduces the synoptic scale meteorology over the
209 Indian region, justifying its use for atmospheric chemical simulations (e. g. Kumar et al., 2012a). Further, nudging
210 towards reanalysis data limits deviations in simulated meteorology (e. g. Kumar et al., 2012a; Ojha et al., 2016;
211 Girach et al., 2017). Nevertheless, we include an evaluation of model simulated water vapour, temperature and
212 wind speed against radiosonde observations (Supplementary material, Fig. S3). Vertical profiles of the monthly
213 average (April) water vapour mixing ratio (g/Kg), temperature (^{o}C) and horizontal wind speed (m/s) have been
214 obtained from radiosonde data (available at http://weather.uwyo.edu/upperair/sounding.html) for evaluation of
215 modelled meteorology over Delhi (in North India), Bhubaneshwar (in east India) and Ahmedabad (in west India).
216 We find that model simulated meteorology is in good agreement (within 1-standard deviation variability) with the
217 observations.
218
219 Surface ozone data is acquired from various studies and sources, as given in Table 4. In general, surface O_3
220 measurements over these stations have been conducted using the well-known technique of UV light absorption by
221 ozone molecules at about 254 nm, making use of Beer-Lambert's Law. The accuracy of these measurements is
222 reported to be about 5% (Kleinmann et al., 1994). The response time of such instruments is about 20 s and
223 instruments have a lower detection limit of 1 ppbv (Ojha et al., 2012). Here we have used the hourly and monthly
224 average data for the model evaluation. The details of instruments and calibrations at individual stations can be
225 found in the references given in the Table 4.

226 As simultaneous measurements at different stations are very sparse over South Asia, the model evaluation has
227 often to be conducted using observations of the same season/month of a different year (e. g. Kumar et al., 2012b;
228 Kumar et al., 2015; Ojha et al., 2016). However, to minimize the effect of temporal differences we preferentially
229 used measurements of recent years i.e. the observations at ~83% of the stations used in this study are of the period:
230 2009-2013. For four stations: Delhi (north India), Jabalpur (central India), Pune (west India) and Thumba (south
231 India), the observations and simulations are for the same year (2013). The observations at three stations have been
232 collected in previous periods (2004 or before). Finally, we investigated the effects of temporal differences on the
233 results and model biases presented here by conducting another simulation for a different year (2010)
234 (Supplementary material, Fig. S4).

235 There is also a need to evaluate precursor mixing ratios over the region to further reduce uncertainties in modelled
236 ozone over South Asia. However, very limited data is available for ozone precursors in India and adjacent

countries (especially for non-methane volatile organic compounds; NMVOCs). We include an evaluation of modelled NOx, ethane and ethene mixing ratios against several recent observations. For this the reader is directed to the supplementary material (Section S1 and Table S1 on Pages: 1-2 in the supplement).

3. Effects of emission inventories

3.1. Spatial distribution of Ozone

The spatial distribution of WRF-Chem simulated 24-h monthly average ozone during April is shown in Fig. 3a (upper panel) for the three different emission inventories (HTAP, INTEX, and SEAC4RS). Generally the months of March and May are marked with seasonal transition from winter to summer and summer to monsoon respectively. Hence, the month of April is chosen to represent the pre-monsoon season as it is not influenced by these seasonal transitions, and the observational data is available for a maximum number of stations during this month for the comparison. The 24-h average ozone mixing ratios are found to be 40-55 ppbv over most of the Indian subcontinent for all the three inventories. Model simulated ozone levels over the coastal regions are also similar (30-40 ppbv) among the three inventories. The highest ozone mixing ratios (55 ppbv and higher) predicted in the South Asian region are found over northern India and the Tibetan Plateau. The WRF-Chem simulated spatial distributions of average ozone shown here are in agreement with a previous evaluation study over South Asia (Kumar et al., 2012b). Further, it is found that qualitatively as well as quantitatively the HTAP, INTEX-B and SEAC4RS lead to very similar distributions of 24-h average ozone over most of the South Asian region. The 24h monthly average ozone from observations is superimposed on the model results in Fig. 3a for comparison. WRF-Chem simulated distributions of average O_3 are in general agreement with the observational data (Fig. 3a), except at a few stations near coasts (e. g. Kannur and Thumba) and in complex terrain (Pantnagar and Dibrugarh). In contrast to the distribution of 24-h average O_3, the noontime (1130-1630 IST) O_3 mixing ratios over continental South Asia exhibit significant differences among the three emission inventories (Fig. 3b). HTAP clearly leads to higher noontime O_3 mixing ratios, the difference being up to 10 ppbv over the Indo-Gangetic plain (IGP), 20 ppbv over Central India, and 30 ppbv over Southern India, compared to INTEX-B and SEAC4RS. The mean bias (MB) (model-observation) for 24-h and noontime average ozone at individual stations is provided in the supplementary material - Table S2 and S3. A sensitivity simulation is conducted to reveal the influence of a different cumulus parameterization (Kain-Fritsch scheme) on our conclusions. The differences in the modelled surface ozone mixing ratios over most of the Indian domain are found to be within ±5% (supplementary material; Figure S5). The relatively large differences over some of the Indian region indicate that the Kain-Fritsch scheme tends to predict higher surface ozone mixing ratios relative to the base run (incorporating Grell 3D Ensemble Scheme) which would only add up to biases in the original runs. Therefore our conclusions are not affected.

The net photochemical O_3 production rate (ppbv h^{-1}) from sunrise to noontime (0630-1230 IST), when most of the photochemical build-up of ozone takes place leading to its peak noontime mixing ratio, has been calculated utilizing the chemical tendencies in WRF-Chem (Barth et al., 2012; Girach et al., 2017). A comparison of monthly average O_3 production rates among the three inventories is shown in Fig. 4. As seen also from the O_3 mixing ratios (Fig. 3b), the HTAP emissions result in faster O_3 production (~9 ppbv h^{-1}) throughout the IGP region. The highest O_3 production rates for INTEX-B and SEAC4RS inventories are simulated only in the East Indian regions including the eastern parts of the IGP. It is noted that the rate of O_3 production is lower (4-8 ppbv h^{-1}) over most of

the south-western IGP for the INTEX-B and SEAC4RS inventories. Differences are also found over the southern Indian region with stronger ozone production in HTAP, followed by INTEX-B and SEAC4RS.

Figure 5 provides insight into the spatial distribution of O_3 production regimes estimated through the CH_2O/NO_y ratio (Geng et al., 2007; Kumar et al. 2012b) calculated during 0630 – 1230 IST, to help explain the differences in modelled ozone mixing ratios among the three simulations. An explanation for why the metric CH_2O/NO_y is a more useful diagnostic to determine ozone production regime than by simply analysing the NO_x and NMHC loadings is found in Sillman (1995). A value of 0.28 for CH_2O/NO_y ratio is suggested to be the transitional value from VOC limited regime to NO_x limited regime. The spatial distribution of regimes in all simulations in the present study is largely consistent with the findings of Kumar et al. (2012b) although the latter performed the analysis for afternoon hours (1130 – 1430 IST). The S4RS-RADM2 simulation predicts the entire IGP to be VOC sensitive whereas in HTAP-RADM2 and INTEX-RADM2 simulations though the northwest IGP and eastern IGP are VOC sensitive, the central IGP is mostly NO_x limited. The coastal regions are also predicted to be VOC limited in all the three simulations. With the north-western IGP being VOC limited in all simulations, the noontime ozone mixing ratios are found to be higher in this region in HTAP-RADM2 simulation because of high NMVOC emissions in HTAP inventory as evident from figure 2 and table 2. Similar differences are also apparent in southern India.

In summary, these results show similar 24-h average ozone distributions but large differences in the ozone build-up until noon. The net photochemical ozone production in the morning hours (0630-1230) is shown to be sensitive to the different inventories over this region, which is attributed to differences in total NO_x and/or NMVOC emissions. We therefore suggest that a focus on 24-h averages only would be insufficient to evaluate the ozone budget and implications for human health and crop yield. Next we compare the modeled diurnal ozone variations from three inventories with in situ measurements over 18 stations across the South Asia.

3.2. Diurnal variation

A comparison of WRF-Chem simulated diurnal ozone variability with recent in situ measurements over a network of 18 stations in the South Asian region is shown in Fig. 6. WRF-Chem is found to successfully reproduce the characteristic diurnal ozone patterns observed over the urban (e.g. Mohali, Delhi, Kanpur, Ahmedabad, Bhubaneswar and Pune) and rural (e.g. Joharapur, Anantpur, Gadanki) stations, indicating strong ozone build-up from sunrise to noontime and the predominance of chemical titration (by NO) and deposition losses during the night. In general, WRF-Chem captures the daily amplitude of O_3 changes at relatively cleaner and high altitude stations, typically showing less pronounced diurnal variability, such as Nainital in the Himalayas and Mt. Abu in the Aravalli mountain range, although with differences in timing when model and observations attain minimum ozone mixing ratios, thus leading to relatively low correlation coefficient (see later in the text). For example, modelled diurnal amplitudes at Nainital are estimated to be ~19.2 ppbv (HTAP-RADM2), ~17.5 ppbv (INTEX-RADM2) and ~17.9 ppbv (S4RS-RADM2) as compared to the observational value of ~15.1 ppbv. The model does not reproduce the ozone mixing ratios at Pantnagar and Jabalpur except for afternoon peak values. This can be attributed to the role of complex terrain (presence of the Himalayas near Pantnagar), which cannot be fully resolved, even at 12 km resolution. Jabalpur is also surrounded by forests, hills and mountains (Sarkar et al., 2015), and such variability in a small area could impact the accuracy of model predictions. The model typically

overestimates the noontime ozone mixing ratios over several urban (e.g. Kanpur, Ahmedabad, Haldia, Thumba) and rural stations (e.g. Joharapur, Kannur), which is attributed to the uncertainties in the emissions.

To briefly evaluate the possible effects due to the difference in meteorological year between model and observations, we repeated the HTAP-RADM2 simulation for a different year (2010) as shown in the Supplementary material – Fig. S4. The effect of changing the meteorological year in the model simulation is generally small (mostly within ±3 ppbv in 3 years), except at a few stations in the east (Haldia and Bhubaneswar) and north (Nainital and Pantnagar). The effect is seen to vary from 4.8 ppbv to 11 ppbv (in 3 years) at these four stations. These differences are found to be associated with the inter-annual variations in the regional and transported biomass burning emissions, as seen from MODIS fire counts and MOZART/GEOS5 boundary conditions (not shown).

The model ability to reproduce diurnal variations at all stations is summarised using a Taylor diagram (Taylor, 2001) in Figure 7. The statistics presented are normalised standard deviation (SD), normalised centred root mean squared difference (RMSD) and the correlation coefficient. The normalisation of both SD and RMSD is done using the standard deviation of the respective observational data. The point indicated as 'REF' represents the observational data against the model results evaluated. WRF-Chem simulations show reasonable agreement with observations showing correlation coefficients generally greater than 0.7 for most sites. The locations such as Nainital, Mt. Abu and Jabalpur for which r values are lower (0.3-0.7) are associated with unresolved complex terrain, as mentioned earlier. Note that the Taylor diagram has been used to present evaluation statistics for a general overview and inter-comparison i.e. how the model reproduces the diurnal variation at different stations, irrespective of the emission inventory.

4. Effects of chemical mechanism (RADM2 vs MOZART)

A recent WRF-Chem evaluation over Europe showed better agreement with in situ measurements when the MOZART chemical mechanism was employed, compared to RADM2 (Mar et al., 2016). Following up on this, here we compare modelled ozone mixing ratios obtained with these two extensively used chemical mechanisms over South Asia: RADM2 (e. g. Michael et al., 2013; Ojha et al., 2016, Girach et al., 2017) and MOZART (e. g. Ghude et al., 2014; Ghude et al., 2016), keeping the same input emission inventory (HTAP). Thus, the following sensitivity analysis is aimed at exploring if the use of the more detailed chemical mechanism of MOZART could improve the model performance.

4.1. Spatial distribution of surface O_3

The WRF-Chem simulated spatial distributions of 24-h average and noontime average surface ozone are compared in Fig. 8. The monthly values of the 24-h and noontime ozone mixing ratios from measurements are also shown. Overall, the average ozone mixing ratios over South Asia are simulated to be higher with the MOZART chemical mechanism compared to RADM2, which is consistent with the results of Mar et al. (2016) for the European domain. The 24-h average ozone mixing ratios over India simulated with MOZART chemistry are found to be higher than those with RADM2 chemistry, especially over the eastern Indian region (~60 ppbv and more for MOZART compared to ~40-55 ppbv for RADM2). Average ozone levels over the coastal regions are found to be similar between the two mechanisms (30-40 ppbv). MOZART chemistry also predicts high 24-h average ozone mixing ratios (55 ppbv and higher) over the Tibetan Plateau region, similar to RADM2. A striking difference between the two chemical mechanisms is found over the marine regions adjacent to South Asia (Bay of Bengal

and northern Indian Ocean), with MOZART predicting significantly higher 24-h average ozone levels (35-50 ppbv) compared to the RADM2 (25-40 ppbv). A comparison of noontime average ozone distributions between the two chemical mechanism shows that MOZART predicts higher ozone concentrations than RADM2 over most of the Indian region by about 5-20 ppbv, except over western India. The differences are up to 20 ppbv and more over the Southern Indian region, highlighting the impacts of chemical mechanisms on modelled ozone in this region. The mean bias (MB) values (model-observation) for 24-h and noontime average ozone at individual stations is provided in the supplementary material - Table S2 and S3.

Figure 9a shows a comparison of the monthly average chemical O_3 tendency (ppbv h^{-1}) from 0630 to 1230 IST. In contrast with average O_3 mixing ratios, which were found to be higher in HTAP-MOZ, the net O_3 production rates at the surface are higher in HTAP-RADM2 over most of the domain, especially in the IGP and central India. The net O_3 production rates at the surface with HTAP-RADM2 are found to be 6 to 9 ppbv $h^{-1}$and more over the IGP, whereas these values are generally lower in HTAP-MOZ (4-8 ppbv h^{-1}), except in the north-eastern IGP (>9 ppbv h^{-1}). Fig. 9b shows the sum of the chemical tendency and vertical mixing tendency at the surface for the HTAP-RADM2 and HTAP-MOZ. Analysis of the vertical mixing tendency revealed that higher surface ozone mixing ratios in the MOZART simulation are due to mixing with ozone rich air from aloft. In the HTAP-RADM2 simulation, vertical mixing dilutes the effect of strong chemical surface ozone production. Further analysis of vertical distributions of chemical O_3 tendencies reveals stronger photochemical production of ozone aloft with MOZART compared to RADM2 (Supplementary material-Fig. S6). This leads to higher ozone mixing ratios aloft in MOZART simulations. A sensitivity simulation is conducted using a different PBL parameterization (Yonsei University Scheme) to examine its influence on our conclusions. Comparison of monthly average (in April) planetary boundary layer heights between the two PBL schemes revealed that the differences are mostly within ±150 m with Yonsei scheme generally resulting in higher PBL heights over India (Fig. S8). Nevertheless, the chemical tendencies combined with vertical mixing tendencies of surface O_3 are found to be nearly similar with Yonsei scheme (Fig. S9) as in the base runs using the MYJ scheme (Fig. 9b in manuscript) with MOZART still producing higher ozone aloft (not shown) as in the original runs. Thus changing the PBL scheme still results in production of more ozone aloft in MOZART, which is getting mixed with near surface air, which corroborates that our conclusions are not affected.

Mar et al. (2016) showed that RADM2 exhibits greater VOC sensitivity than MOZART (i.e., producing higher changes in ozone given a perturbation in VOC emissions) under noontime summer conditions over Europe. This is consistent with our findings as well, that the net surface photochemical ozone production is greater for HTAP-RADM2 than for HTAP-MOZART, given the high VOC emissions in the HTAP inventory. At the surface, the MOZART mechanism predicts larger areas of VOC-sensitivity (as diagnosed by the CH_2O/NO_y indicator, Figure 10) and lower net photochemical ozone production than RADM2. With increasing altitude, both the HTAP-RADM2 and HTAP-MOZART simulations show a general increase of CH_2O/NO_y over India, i.e. the chemistry tends to exhibit increased NO_x sensitivity with increasing height (Supplementary material-Figure S10). At model levels above the surface, HTAP-MOZART shows greater net photochemical production of ozone than HTAP-RADM2 (Supplementary material-Figure S6), which is what Mar et al. (2016) have also reported for the surface O_3 over Europe. When these effects are combined, mixing leads to higher surface ozone mixing ratios for HTAP-MOZART than for HTAP-RADM2. A sensitivity simulation using a different photolysis scheme (Madronich TUV photolysis scheme) with HTAP-RADM2 setup revealed similar surface ozone mixing ratios and chemical

tendencies at various model levels with small differences (<5%) over most of the Indian region (not shown). So our results would be similar if we use Madronich TUV scheme instead of Fast-J scheme with RADM2. Further, Mar et al. (2016) used Madronich TUV scheme with RADM2 and Madronich F-TUV scheme with MOZART chemical mechanism and reported that the two different Madronich photolysis schemes had only a small contribution to the differences in the predicted ozone by two chemical mechanisms. The major difference between the two chemical mechanisms was due to differences in inorganic reaction rates (Mar et al, 2016). Hence we conclude that in our study too, the differences over Indian region are primarily due to the choice of the chemical mechanisms irrespective of photolysis scheme used. Also note that the aerosol radiation feedback is turned off, so that the calculated differences mainly result from the representation of gas phase chemistry rather than of aerosols between MOZART and RADM2. Our analysis also shows the importance of chemical regime in understanding differences between the chemical mechanisms, and highlights the significant effects of the employed chemical mechanism on modelled ozone over South Asia.

4.2. Diurnal variation

Figure 11 shows a comparison of WRF-Chem simulated ozone variations on diurnal timescales with recent in situ measurements over a network of stations across the South Asia for the two chemical mechanisms (MOZART and RADM2); again with the same emission inventory (HTAP). Qualitatively, both simulations produce very similar diurnal patterns, however, the absolute O_3 mixing ratios are found to differ significantly between the two chemical mechanisms. Noontime ozone mixing ratios predicted by MOZART are either significantly higher (at 12 out of 18 stations) or nearly similar (at 6 stations). MOZART-predicted O_3 at Dibrugarh, Kanpur, Jabalpur, Bhubaneshwar, Gadanki and Thumba was found to be higher by ~12 ppbv, 5 ppbv, 8 ppbv, 10 ppbv, 11 ppbv and 12 ppbv, respectively, compared to RADM2 (Supplementary material, Table S3). Over several urban and rural stations in India (e.g. Delhi, Ahmedabad, Pune, Kannur and Thumba) MOZART is found to titrate ozone more strongly during the night while resulting in higher or similar ozone levels around noon. The contrasting comparison between noon and night time found at these sites suggests that evaluation limited to 24 h averages would not be sufficient, and that model performance on a diurnal time scale should be considered to assess the photochemical build-up of O_3.

In general, the noontime ozone mixing ratios predicted by RADM2 are found to be in better agreement with in situ measurements compared to MOZART. The model performance of two chemical mechanisms in reproducing diurnal variation at all stations is summarised using a Taylor diagram in Fig. 12. Both chemical mechanisms show reasonably good agreement ($r > 0.7$) at most of the sites, except two stations associated with highly complex terrain (Nainital and Mt. Abu). On the Taylor diagram, most of the HTAP-RADM2 results are found to be closer to the 'REF', as compared to HTAP-MOZ results, suggesting that the RADM2 chemical mechanism is better suited to simulate ozone over this region.

5. Overall evaluation and recommendations

In this section, we present a sub-regional evaluation of all simulations by subdividing the domain into five geographical areas, i.e. North, South, East, West and central India, as shown in Fig. 1. The recommendations for the individual stations based on the model evaluation are summarized in the Supplementary material (Table S2 and S3). The temporal correlation coefficients of diurnally varying O_3, spatially averaged over each of the five

different sub-regions, are found to be reasonably high, generally exceeding 0.7 (Table 5). The r values for individual sub-regions are found to be similar among the four simulations. For example, over north India the r values vary from 0.86 to 0.90. The model performance differs among several sub-regions, with correlations being lower for central India (r = 0.67-0.75). Since the latter is based on only one station associated with complex terrain (Jabalpur), we suggest that observations over additional stations should be conducted to evaluate the model performance in the central Indian region. As correlations are similar among different simulations, we focus on the mean bias values especially around noontime (Table 6). Amongst the four different combinations of simulations performed we find HTAP-RADM2 yields lowest noontime biases over north (MB = ~2.4 ppbv) and central India (~0.9 ppbv). The S4RS-RADM2 combination is recommended for the east (MB ~15.3 ppbv) and South (MB ~6.5 ppbv) Indian regions. On the other hand, INTEX-RADM2 is found to yield better agreement with measurements over western India (MB = ~8 ppbv). The recommendation for each region based solely on the ability to predict noontime O_3 concentrations is summarized in table 7. These results show that the performance of emission inventories is regionally different, and that these biases should be considered in utilizing model for assessment of air quality and impacts on human health and crop yield.

We finally evaluate the different simulations in the context of the entire south Asian region. Figure 13 shows a comparison of model results and measurements with diurnal box/whisker plots, combining all stations for the four different simulations. As mentioned earlier, noontime ozone levels are overestimated by all four simulations. The overestimation of noontime ozone is found to be largest in the HTAP-MOZ simulation, followed by HTAP-RADM2, and lowest with S4RS-RADM2. These results further suggest that assessment of the tropospheric ozone budget as well as implications for public health and crop loss are associated with considerable uncertainty, and biases need to be considered. A recent study (Ghude et al., 2016), for example, subtracted 15 ppbv from the WRF-Chem simulated ozone mixing ratios before deriving premature mortalities over the Indian region. The results of this study are summarized in the form of a polar plot (Fig. 14) showing the monthly mean diurnal variation from all runs for the entire south Asian domain. The noontime normalized mean bias values with respect to observed values are ~11% (S4RS-RADM2), ~12.5% (INTEX-RADM2), ~22% (HTAP-RADM2) and ~36.5% (HTAP-MOZ). It is interesting to note that the SEAC4RS inventory (representative of year 2012) yields quite similar domain wide average bias value as the INTEX-B inventory (representative of year 2006). It is concluded that the SEAC4RS inventory, which is the most recent inventory amongst the three inventories considered in this study, is best suited for O_3 prediction over south Asian region as a whole in combination with RADM2 Chemistry.

6. Summary and conclusions

In this paper, we evaluated the WRF-Chem simulated surface ozone over South Asia during the pre-monsoon season against recent in situ measurements from a network of 18 stations, employing three different inventories (EDGAR-HTAP, INTEX-B, and SEAC4RS) for anthropogenic emissions with the RADM2 chemical mechanism. WRF-Chem simulated ozone distributions showed highest ozone mixing ratios (~55 ppbv and higher) over northern India and the Tibetan Plateau. In general, modelled average ozone distributions from different inventories are found to be in agreement with previous studies over this region. Evaluation on diurnal time scales demonstrates the ability of the model to reproduce observed O_3 patterns at urban and rural stations, showing strong noontime ozone build-up and chemical titration and deposition loss during the night-time. WRF-Chem also captures the smaller diurnal amplitudes observed over high altitude, relatively pristine stations. However, model

showed limitations in capturing ozone mixing ratios in the vicinity of the complex terrain, indicating that even a relatively high horizontal resolution of 12 km x 12 km could not fully resolve the topography induced effects.

Overall WRF-Chem simulations show reasonable agreement with observations, with correlation coefficients generally higher than 0.7 for most of the sites. It is found that the HTAP, INTEX-B and SEAC4RS inventories lead to very similar distributions of 24-h average ozone over this region. This is corroborated by the quantitative similarity in simulated surface ozone among the three simulations, for both 24h and noontime (1130-1630 IST) averages at all grids in the domain (supplementary material, table S5). However, noontime (1130-1630 IST) O_3 mixing ratios over continental South Asia differ significantly among the three inventories. This can also be seen in the quantitative assessment of similarity (Table S5), where the variance of the residual shows that the scatter is greater for the noontime averages than for the 24 h averages. HTAP inventory generally leads to noontime O_3 mixing ratios higher by 10 ppbv over the Indo-Gangetic plain (IGP), 20 ppbv over Central India, and 30 ppbv over Southern India, compared to the INTEX-B and SEAC4RS inventories. A comparison of monthly average O_3 net production rate during 0630-1230 IST among the three inventories shows that the HTAP emissions result in faster O_3 production (~9 ppbv h^{-1}) throughout the IGP region compared to the other two inventories. Differences are also found over the southern Indian region with stronger ozone production in HTAP, followed by INTEX-B and SEAC4RS. The results show similar 24-h average ozone distributions, but large differences in noontime ozone build up, pointing to the uncertainties in emission inventories over this region.

We further investigated the sensitivity of modelled ozone to two extensively used chemical mechanisms, RADM2 and MOZART, and maintaining the HTAP emissions. Noontime average surface ozone distributions predicted by MOZART show significant enhancements (10-15 ppbv) with respect to RADM2 over most of the Indian region, except over western India. MOZART predicts higher ozone concentrations than RADM2 by up to 20 ppbv and more over the South Indian region. Monthly average ozone mixing ratios are predicted to be higher by the MOZART chemical mechanism compared to RADM2, as was also found over Europe (Mar et al., 2016). The differences in ozone production between the MOZART and RADM2 chemical mechanisms are mainly attributed to the additional chemical species and reactions, differences in the rate constants for several inorganic reactions, and photolysis schemes used. A comparison of the monthly average chemical O_3 tendency (ppbv h^{-1}) during 0630-1230 IST shows that in contrast with average O_3 mixing ratios, which were found to be higher in MOZART, the net O_3 production rates at the surface are higher with RADM2 chemistry, especially over the IGP and central India. The net O_3 production rates at the surface with RADM2 are found to be 6 to 9 ppbv h^{-1}, and higher over the IGP, whereas these rates are generally lower with MOZART (4-8 ppbv h^{-1}), except in the northeastern IGP (>9 ppbv h^{-1}). Analysis of the vertical mixing tendency revealed that higher surface ozone mixing ratios in the MOZART simulation are due to mixing with ozone rich air from aloft. Analysis of vertical distributions of chemical O_3 tendencies reveals stronger photochemical production of ozone aloft with MOZART compared to RADM2. Our analysis highlights the significant effects of the employed chemical mechanism on model predicted ozone over South Asia.

Qualitatively, RADM2 and MOZART simulations predict similar diurnal patterns; however the absolute O_3 mixing ratios differ significantly. Noontime ozone mixing ratios predicted by MOZART are significantly higher at 12 out of 18 stations, while these were found to be similar at 6 stations. Over several urban and rural stations in India MOZART is found to titrate ozone relatively strongly during the night, while producing higher or similar

ozone levels during noontime compared to RADM2. The contrasting evaluation results between day- (noon) and night-time could counterbalance in evaluation studies limited to 24 h averages, possibly showing better agreement and therefore hence it is pertinent to consider the diurnally resolved model performance. In general, the noontime ozone mixing ratios predicted by RADM2 are found to be in better agreement with in situ measurements at the surface compared to MOZART.

Model evaluation over different geographical regions in South Asia reveals strong spatial heterogeneity in the WRF-Chem performance. SEAC4RS inventory leads to better agreement with observations over east (MB = ~15.3 ppbv) and south India (~6.5 ppbv), whereas the HTAP inventory performs better over north (MB = ~2.4 ppbv) and central India (~0.9 ppbv), and INTEX-B over west India (MB = ~8 ppbv). For the entire region, the overestimation of noontime ozone is found to be highest with the HTAP inventory (with the MOZART chemical mechanism) and lowest with the SEAC4RS inventory. The noontime normalized mean bias is lowest for the SEAC4RS inventory with the RADM2 chemical mechanism (~11%), followed by INTEX-B with RADM2 (~12.5%), HTAP with RADM2 (~22%), and HTAP with MOZART (~36.5%). These results further suggest that the assessment of the tropospheric ozone budget and consequently its implications on public health and agricultural output should be carried out cautiously by considering the large uncertainties associated with use of emission inventories and chemical mechanism incorporated. It is interesting to note that the SEAC4RS inventory (representative of 2012) yields results comparable to the INTEX-B inventory (for 2006), even though the SECA4RS inventory has about 46% higher NO_x, 9% higher NMVOC and 15% lower CO emissions compared to INTEX-B. We conclude that the SEAC4RS inventory, the most recent inventory amongst the three inventories, is best suited for O_3 prediction over south Asian region as a whole in combination with RADM2 Chemistry.

Brown carbon aerosol can effectively absorb solar radiation (Alexander et al., 2008; Hecobian et al., 2010; Kirchstetter and Thatcher, 2012; Kirchstetter et al., 2004; Yang et al., 2009; Jo et al., 2016) leading to a reduction in NO_2 photolysis rates and subsequently in surface ozone mixing ratios (Jo et al., 2016). Jo et al. (2016) reported that on an annual average basis, changes in surface ozone mixing ratios related to brown carbon aerosol absorption over South Asia are <5%. Further studies should be taken up in the future to investigate the impact of aerosols on surface ozone, also with regional models like WRF-Chem. The current and other modelling efforts, constrained by limited measurement data, stress the need for more comprehensive observations, e.g. in a network of stations, and making the data available through projects such as TOAR (http://toar-data.fz-juelich.de/). Our study highlights the need to also evaluate O_3 precursors, similar to that conducted here for ozone, to further reduce uncertainties in modelled ozone over South Asia for the better assessment of implications of surface ozone on public health and crop yield. We also recommend preparing high-resolution regional inventories for the anthropogenic emissions of O_3 precursors over South Asia, also accounting for year-to-year changes.

Data availability: The model output from all the numerical simulations is available at the MPG supercomputer HYDRA (http://www.mpcdf.mpg.de/services/computing/hydra) and would be provided by contacting the corresponding authors. The observed values shown for comparison are from previous papers with complete list of references provided in the Table 4. New observations for Delhi and Pune stations are available from the SAFAR program (http://safar.tropmet.res.in/).

Acknowledgement

A. Sharma acknowledges the fellowship from the Max Planck Institute for Chemistry to carry out this study. S. S. Gunthe acknowledges the support from DST-Max Planck partner group at IIT Madras and Ministry of Earth Sciences (MoES), Govt. of India. Model simulations have been performed on the MPG supercomputer HYDRA (http://www.mpcdf.mpg.de/services/ computing/hydra). Initial and boundary conditions data for meteorological fields were obtained from ECMWF website (http://www.ecmwf.int/en/research/climate-reanalysis/era-interim). The HTAP v2 anthropogenic emissions were obtained from http://edgar.jrc.ec.europa.eu/htap_v2/index.php?SECURE=123. Authors are grateful to Yafang Cheng (MPI-C) for providing SEAC4RS emission. The INTEX-B anthropogenic emissions were obtained from http://bio.cgrer.uiowa.edu/EMISSION_DATA_new /data/intex-b_emissions/. MOZART-4/ GEOS5 output used as initial and boundary conditions for chemical fields is acknowledged. The pre-processors and inputs for biogenic and biomass-burning emissions were obtained from NCAR Atmospheric Chemistry website (http://www.acd.ucar.edu/wrf-chem/). Radiosonde data of water vapour mixing ratio, temperature and wind speed were obtained from University of Wyoming website (http://weather.uwyo.edu/upperair/sounding.html). Authors are also thankful for the usage of HPC supercluster and to the staff at P. G. Senapathy Computer Center at IIT Madras. Constructive comments and suggestions from two anonymous reviewers are gratefully acknowledged.

References

Ackermann, I. J., Hass, H., Memmesheimer, M., Ebel, A., Binkowski, F. S., and Shankar, U.: Modal aerosol dynamics model for Europe: development and first applications, Atmos. Environ., 32, 2981–2999, doi:10.1016/S1352-2310(98)00006-5, 1998.

Ainsworth, E. A., Yendrek, C. R., Sitch, S., Collins, W. J., and Emberson, L. D.: The effects of tropospheric ozone on net primary productivity and implications for climate change, Ann. Rev. Plant Biol., 63, 637–661, 2012.

Akimoto, H.: Global air quality and pollution, Science, 302, 1716–1719, doi:10.1126/science.1092666, 2003.

Amnuaylojaroen, T., Barth, M. C., Emmons, L. K., Carmichael, G. R., Kreasuwun, J., Prasitwattanaseree, S., and Chantara, S.: Effect of different emission inventories on modeled ozone and carbon monoxide in Southeast Asia, Atmos. Chem. Phys., 14, 12983-13012, doi:10.5194/acp-14-12983-2014, 2014.

Anenberg, S. C., Horowitz, L. W., Tong, D. Q., and West, J. J.: An estimate of the global burden of anthropogenic ozone and fine particulate matter on premature human mortality using atmospheric modelling, Environmental Health Perspectives, 118, 1189–1195, 2010.

Ansari, T. U., Ojha, N., Chandrasekar, R., Balaji, C., Singh, N. and Gunthe, S. S.: Competing impact of anthropogenic emissions and meteorology on the distribution of trace gases over Indian region, J. Atmos. Chem., doi:10.1007/s10874-016-9331-y, 2016.

Atkinson, R.: Atmospheric chemistry of VOCs and NOx, Atmos. Environ., 34, 2063–2101, doi:10.1016/S1352-2310(99)00460-4, 2000.

588 Barth, M. C., Lee, J., Hodzic, A., Pfister, G., Skamarock, W. C., Worden, J., Wong, J., and Noone, D.:
589 Thunderstorms and upper troposphere chemistry during the early stages of the 2006 North American Monsoon,
590 Atmos. Chem. Phys., 12, 11003-11026, doi:10.5194/acp-12-11003-2012, 2012.

591 Bell, M. L., McDermott, A., Zeger, S. L., Samet, J. M., and Dominici, F.: Ozone and short term mortality in 95 US
592 urban communities, 1987-2000, JAMA The Journal of the American Medical Association, 292, 2372-2378, 2004.

593 Bhuyan, P.K., Bharali, C., Pathak, B., and Kalita, G.: The role of precursor gases and meteorology on temporal
594 evolution of O3 at a tropical location in northeast India, Environmental Science and Pollution Research, 21, 6696–
595 6713, 2014.

596 Carmichael, G. R., Sakurai, T., Streets, D., Hozumi, Y., Ueda, H., Park, S. U., Funge, C., Han, Z., Kajino, M.,
597 Engardt, M., Bennet, C., Hayami, H., Sartelet, K., Holloway, T., Wang, Z., Kannari, A., Fu, J., Matsuda, K.,
598 Thongboonchoo, N., and Amann, M.: MICS-Asia II: the model intercomparison study for Asia Phase II
599 methodology and overview of findings, Atmos. Environ., 42, 3468–3490, doi:10.1016/j.atmosenv.2007.04.007,
600 2008.

601 Chin, M., Rood, R. B., Lin, S. -J., Muller, J. F., and Thomspon, A. M.: Atmospheric sulfur cycle in the global
602 model GOCART: Model description and global properties, J. Geophys. Res., 105, 24,671-24,687, 2000.

603 Chou, M. -D., and Suarez, M. J.: An efficient thermal infrared radiation parameterization for use in general
604 circulation models, NASA Technical Memorandum 104606, 3, 85pp, 1994.

605 Cox, R. A., Eggleton, A. E. J., Derwent, R. G., Lovelock, J. E., and Pack, D. H.: Long-range transport of
606 photochemical ozone in north-western Europe, Nature, 255, 118 – 121, doi:10.1038/255118a0, 1975.

607 Crutzen, P. J.: Photochemical reactions initiated by and influencing ozone in unpolluted tropospheric air, Tellus,
608 26, 47–57, 1974.

609 David, L. M., and Nair, P. R.: Diurnal and seasonal variability of surface ozone and NOx at a tropical coastal site:
610 association with mesoscale and synoptic meteorological conditions, Journal of Geophysical Research 116,
611 D10303. http://dx.doi.org/10.1029/2010JD015076, 2011.

612 Debaje, S. B., and Kakade, A. D.: Measurements of Surface Ozone in Rural Site of India, Aerosol and Air Quality
613 Research, Vol. 6, No. 4, pp. 444-465, 2006.

614 Dumka, U. C., Krishna Moorthy, K., Kumar, R., Hegde, P., Sagar, R., Pant, P., Singh, N., and Suresh Babu, S.:
615 Characteristics of aerosol black carbon mass concentration over a high altitude location in the central Himalayas
616 from multi-year measurements, Atmos. Res., 96, 510–521, 2010.

617 Emberson, L. D., Buker, P., Ashmore, M., Mills, G., Jackson, L., Agrawal, M., Atikuzzaman, M., Cinderby, S.,
618 Engardt, M., Jamir, C., Kobayashi, K., Oanh, N., Quadir, Q., and Wahid, A.: A comparison of North-American
619 and Asian exposure-response data for ozone effects on crop yields, Atmos. Environ., 43, 1945–1953, 2009.

620 Emmons, L. K.,Walters, S., Hess, P. G., Lamarque, J.-F., Pfister, G. G., Fillmore, D., Granier, C., Guenther, A.,
621 Kinnison, D., Laepple, T., Orlando, J., Tie, X., Tyndall, G., Wiedinmyer, C., Baughcum, S. L., and Kloster, S.:

622 Description and evaluation of the Model for Ozone and Related chemical Tracers, version 4 (MOZART-4),
623 Geosci. Model Dev., 3, 43–67, 20 doi:10.5194/gmd-3-43-2010, 2010.

624 Fast, J. D., Gustafson Jr., W. I., Easter, R. C., Zaveri, R. A., Barnard, J. C., Chapman, E. G., Grell, G. A. and
625 Peckham, S. E.: Evolution of ozone, particulates, and aerosol direct radiative forcing in the vicinity of Houston
626 using a fully-coupled meteorology-chemistry aerosol model, Journal of Geophysical Research, 111, D21305,
627 2006.

628 Gaur, A., Tripathi, S. N., Kanawade, V. P., Tare, V., and Shukla, S. P.: Four-year measurements of trace gases
629 (SO2, NOx , CO, and O3) at an urban location, Kanpur, in Northern India, J. Atmos. Chem., 71, 283–301, 2014.

630 Geng, F., Zhao, C., Tang, X., Lu, G., and Tie, X.: Analysis of ozone and VOCs measured in Shanghai: A case
631 study, Atmos. Environ., 41, 989–1001, 2007.

632 Ghude, S. D., Jena, C., Chate, D. M., Beig, G., Pfister, G. G., Kumar, R., and Ramanathan, V.: Reduction in
633 India's crop yield due to ozone, Geophys. Res. Lett., 41, 51971, doi:10.1002/2014GL060930, 2014.

634 Ghude, S. D., Chate, D. M., Jena, C., Beig, G., Kumar, R., Barth, M. C., PFister, G. G., Fadnavis, S. and Pithani,
635 P.: Premature mortality in India due to PM2.5 and ozone exposure, Geophysical Research Letters, 4650 – 4658,
636 2016.

637 Girach, I. A., Ojha, N., Nair, P. R., Pozzer, A., Tiwari, Y. K., Kumar, K. R., and Lelieveld, J.: Variations in O3,
638 CO, and CH4 over the Bay of Bengal during the summer monsoon season: shipborne measurements and model
639 simulations, Atmos. Chem. Phys., 17, 257-275, doi:10.5194/acp-17-257-2017, 2017.

640 Grell, G.: Prognostic evaluation of assumptions used by cumulus parameterizations, Monthly Weather Review,
641 121, 764-787, 1993.

642 Grell, G., and Devenyi, D.: A generalized approach to parameterizing convection combining ensemble and data
643 assimilation techniques, Geophys. Res. Lett., 29(14), 38–31, 2002.

644 Grell, G. A., Peckham, S. E., McKeen, S., Schmitz, R., Frost, G., Skamarock, W. C. and Eder, B.: Fully coupled
645 'online' chemistry within the WRF model, Atmospheric Environment, 39, 6957–6975, 2005.

646 Gupta, M. and Mohan, M.: Validation of WRF/Chem model and sensitivity of chemical mechanisms to ozone
647 simulation over megacity Delhi, Atmospheric Environment, Volume 122, p. 220-229, 2015.

648 Guenther, A., Karl, T., Harley, P., Wiedinmyer, C., Palmer, P. I., and Geron, C.: Estimates of global terrestrial
649 isoprene emissions using MEGAN (Model of Emissions of Gases and Aerosols from Nature), Atmos. Chem.
650 Phys., 6, 3181–3210, doi:10.5194/acp-6-3181-2006, 2006.

651 Gurjar, B. R., Ravindra, K., and Nagpure, A.S.: Air pollution trends over Indian megacities and their local-to-
652 global implications, Atmospheric Environment, Volume 142, Pages 475–495,
653 http://dx.doi.org/10.1016/j.atmosenv.2016.06.030, 2016.

654 Jain, S. L., Arya, B. C., Kumar, A., Ghude, S. D., and Kulkarni, P. S.: Observational study of surface ozone at
655 New Delhi, India, Int. J. Remote Sens., 26, 3515–3524, 2005.

656 Janjic, Z. I.: The step-mountain eta coordinate model: further developments of the convection, viscous sublayer
657 and turbulence closure schemes, Monthly Weather Review 122, 927–945, 1994.

658 Janjic, Z. I.: The surface layer in the NCEP Eta Model, Eleventh Conference on Numerical Weather Prediction,
659 Norfolk, VA, 19–23 August; American Meteorological Society, Boston, MA, 354–355, 1996.

660 Janjic, Z. I.: Nonsingular Implementation of the Mellor–Yamada Level 2.5 Scheme in the NCEP Meso model,
661 NCEP Office Note, No. 437, 61 pp, 2002.

662 Janssens-Maenhout, G., Crippa, M., Guizzardi, D., Dentener, F., Muntean, M., Pouliot, G., Keating, T., Zhang, Q.,
663 Kurokawa, J., Wankmüller, R., Denier van der Gon, H., Kuenen, J. J. P., Klimont, Z., Frost, G., Darras, S., Koffi,
664 B., and Li, M.: HTAP_v2.2: a mosaic of regional and global emission grid maps for 2008 and 2010 to study
665 hemispheric transport of air pollution, Atmos. Chem. Phys, 15, 11411e11432, http://dx.doi.org/10.5194/acp-15-
666 11411-2015, 2015.

667 Jena, C., Ghude, S. D., Pfister, G. G., Chate, D. M., Kumar, R., Beig, G., Surendran, D., Fadnavis, S., and Lal, D.
668 M.: Influence of springtime biomass burning emissions in South Asia on regional ozone: A model based case
669 study, Atmos. Environ., 100, 37–47, doi:10.1016/j.atmosenv.2014.10.027, 2014.

670 Jena, C., Ghude, S. D., Beig, G., Chate, D. M., Kumar, R., Pfister, G. G., Lal, D. M., Surendran, D. E., Fadnavis,
671 S., and van der, A. R. J.: Inter-comparison of different NOx emission inventories and associated variation in
672 simulated surface ozone in Indian region, Atmos. Environ., 117:61–73, 2015.

673 Jerrett, M., Burnett, R. T., Pope, C. A., III, Ito, K., Thurston, G., Krewski, D., et al.: Long-term ozone exposure
674 and mortality, The New England Journal of Medicine, 360, 1085–1095, 2009.

675 Jo, D. S., Park, R. J., Lee, S., Kim, S.-W., and Zhang, X.: A global simulation of brown carbon: implications for
676 photochemistry and direct radiative effect, Atmos. Chem. Phys., 16, 3413-3432, doi:10.5194/acp-16-3413-2016,
677 2016.

678 Kleinman, L., Lee, Y. -N., Springston, S. R., Nunnermacker, L., Zhou, X., Brown, R., Hallock, K., Klotz, P.,
679 Leahy, D., Lee, J. H., and Newman, L.: Ozone formation at a rural site in the southeastern United States, J.
680 Geophys. Res.-Atmos., 99, 3469–3482, doi:10.1029/93JD02991, 1994.

681 Krupa, S. V., Nosal, M., and Legge, A. H.: A numerical analysis of the combined open top chamber data from the
682 USA and Europe on ambient ozone and negative crop responses, Environmental Pollution, 101, 157–160, 1998.

683 Kumar, R., Naja, M., Venkataramani, S., and Wild, O.: Variations in surface ozone at Nainital: A high-altitude site
684 in the central Himalayas, J. Geophys. Res., 115, D16302, doi:10.1029/2009JD013715, 2010.

685 Kumar, R., Naja, M., Pfister, G. G., Barth, M. C., and Brasseur, G. P.: Simulations over South Asia using the
686 Weather Research and Forecasting model with Chemistry (WRF-Chem): set-up and meteorological evaluation,
687 Geoscientific Model Development, 5, 321-343, 2012a.

688 Kumar, R., Naja, M., Pfister, G. G., Barth, M. C., Wiedinmyer, C., and Brasseur, G. P.: Simulations over South
689 Asia using the Weather Research and Forecasting model with Chemistry (WRF-Chem): chemistry evaluation and
690 initial results, Geoscientific Model Development 5, 619-648, 2012b.

691 Kumar, R., Barth, M. C., Pfister, G. G., Nair, V. S., Ghude, S. D., and Ojha, N.: What controls the seasonal cycle
692 of black carbon aerosols in India?, J. Geophys. Res. Atmos., 120, 7788–7812, doi:10.1002/2015JD023298, 2015.

693 Lal, S.: Trace gases over the Indian region, Indian Journal of Radio and Space Physics, 36, 556–579, 2007.

694 Lawrence, M. G., Rasch, P. J., von Kuhlmann, R., Williams, J., Fischer, H., de Reus, M., Lelieveld, J., Crutzen, P.
695 J., Schultz, M., Stier, P., Huntrieser, H., Heland, J., Stohl, A., Forster, C., Elbern, H., Jakobs, H., and Dickerson,
696 R. R.: Global chemical weather forecasts for field campaign planning: predictions and observations of large-scale
697 features during MINOS, CONTRACE, and INDOEX, Atmos. Chem. Phys., 3, 267-289, doi:10.5194/acp-3-267-
698 2003, 2003.

699 Lawrence, M. G. and Lelieveld, J.: Atmospheric pollutant outflow from southern Asia: a review, Atmos. chem.
700 Phys., 10, 11017–11096, doi:10.5194/acp-10-11017-2010, 2010.

701 Lelieveld, J., and Dentener, F.J.: What controls tropospheric ozone?, J. Geophys. Res., 105, 3531-3551, 2000.

702 Lelieveld, J., Berresheim, H., Borrmann, S., Crutzen, P. J., Dentener, F. J., Fischer, H., Feichter, J., Flatau, P. J.,
703 Heland, J., Holzinger, R., Korrmann, R., Lawrence, M. G., Levin, Z., Markowicz, K. M., Mihalopoulos, N.,
704 Minikin, A., Ramanathan, V., de Reus, M., Roelofs, G. J., Scheeren, H. A., Sciare, J., Schlager, H., Schultz, M.,
705 Siegmund, P., Steil, B., Stephanou, E. G., Stier, P., Traub, M., Warneke, C., Williams, J., and Ziereis, H.: Global
706 air pollution crossroads over the Mediterranean, Science, 298, 794–799, doi:10.1126/science.1075457, 2002.

707 Lelieveld, J., Evans, J. S., Fnais, M., Giannadaki, D., and Pozzer, A.: The contribution of outdoor air pollution
708 sources to premature mortality on a global scale, Nature, 525(7569):367-371, 2015.

709 Lin, Y.-L., R. D. Farley, R. D. and Orville, H. D.: Bulk parameterization of the snow field in a cloud model, J.
710 Clim. Appl. Meteorol., 22, 1065–1092, 1983.

711 Liu, Y., Warner, T. T., Bowers, J. F., Carson, L. P., Chen, F., Clough, C. A., Davis, C. A., Egeland, C. H.,
712 Halvorson, S., Huck Jr., T. W., Lachapelle, L., Malone, R. E., Rife, D. L., Sheu, R., -S., Swerdlin, S. P. and
713 Weingarten, D. S.: The operational mesogamma-scale analysis and forecast system of the U.S. Army Test and
714 Evaluation Command. Part 1: Overview of the modeling system, the forecast products, Journal of applied
715 meteorology and climatology 47, 1077–1092, 2008.

716 Logan, J. A., Staehelin, J., Megretskaia, I. A., Cammas, J.-P., Thouret, V., Claude, H., De Backer, H., Steinbacher,
717 M., Scheel, H.-E., Stubi, R., Frohlich, M., and Derwent, R.: Changes in ozone over Europe: Analysis of ozone
718 measurements from sondes, regular aircraft (MOZAIC) and alpine surface sites, J. Geophys. Res., 117, D09301,
719 doi:10.1029/2011JD016952, 2012.

720 Lu, Z. and Streets, D. G.: The Southeast Asia Composition, Cloud, Climate Coupling Regional Study Emission
721 Inventory, available at: http://bio.cgrer.uiowa.edu/ SEAC4RS/emission.html, 2012.

722 Lüthi, Z. L., Skerlak, B., Kim, S.-W., Lauer, A., Mues, A., Rupakheti, M., and Kang, S.: Atmospheric brown
723 clouds reach the Tibetan Plateau by crossing the Himalayas, Atmos. Chem. Phys., 15, 6007-6021,
724 doi:10.5194/acp-15-6007-2015, 2015.

725 Mahapatra, P. S., Jena, J., Moharana, S., Srichandan, H., Das, T., Roy, C. G., and Das, S. N.: Surface ozone
726 variation at Bhubaneswar and intra-corelationship study with various parameters, J. Earth Syst. Sci. 121, 1163–
727 1175, 2012.

728 Mallik C., Lal, S., and Venkataramani, S.: Trace gases at a semi-arid urban site in western India: variability and
729 inter-correlations, J. Atm. Chem. Vol. 72, p. 143-164, 2015.

730 Mar, K. A., Ojha, N., Pozzer, A., and Butler, T. M.: Ozone air quality simulations with WRF-Chem (v3.5.1) over
731 Europe: model evaluation and chemical mechanism comparison, Geosci. Model Dev., 9, 3699-3728,
732 doi:10.5194/gmd-9-3699-2016, 2016.

733 Marrapu, P., Cheng, Y., Beig, G., Sahu, S. K., Srinivas, R. and Carmichael, G. R.: Air Quality in Delhi during the
734 Commonwealth Games, Atmos. Chem. Phys., 14:10619–10630, 2014.

735 Mellor, G. L., and Yamada, T.: Development of a turbulence closure model for geophysical fluid problems,
736 Reviews of geophysics and space physics 20(4), 851–875, 1982.

737 Michael, M., Yadav, A., Tripathi, S. N., Kanawade, V. P., Gaur, A., Sadavarte, P. and Venkataraman, C.:
738 Simulation of trace gases and aerosols over the Indian Domain: Evaluation of the WRF-Chem model, Atmospheric
739 Chemistry and Physics Discussion, 13, 12287-12336, 2013.

740 Mlawer, E. J., Taubman, S. J., Brown, P. D., Iacono, M. J. and Clough, S. A.: Radiative transfer for
741 inhomogeneous atmosphere: RRTM, a validated correlated-k model for the long-wave, Journal of Geophysical
742 Research 102 (D14), 16663–16682, 1997.

743 Monin, A. S. and Obukhov, A. M.: Basic laws of turbulent mixing in the surface layer of the atmosphere, Contrib.
744 Geophys. Inst. Acad. Sci., USSR 24 (151), 163–187, 1954.

745 Monks, P. S., Archibald, A. T., Colette, A., Cooper, O., Coyle, M., Derwent, R., Fowler, D., Granier, C., Law, K.
746 S., Mills, G. E., Stevenson, D. S., Tarasova, O., Thouret, V., von Schneidemesser, E., Sommariva, R., Wild, O.,
747 and Williams, M. L.: Tropospheric ozone and its precursors from the urban to the global scale from air quality to
748 short-lived climate forcer, Atmos. Chem. Phys., 15, 8889-8973, doi:10.5194/acp-15-8889-2015, 2015.

749 Naja, M., Lal, S., and Chand, D.: Diurnal and seasonal variabilities in surface ozone at a high altitude site Mt Abu
750 (24.6N, 72.7E, 1680 m asl) in India, Atmospheric Environment 37, 4205-4215, 2003.

751 Nishanth, T., Praseed, K. M., Satheesh Kumar, M. K., and Valsaraj, K. T.: Analysis of Ground Level O3 and NOx
752 Measured at Kannur, India. J Earth Sci Climate Change, 3:111, doi:10.4172/2157-7617.1000111, 2012.

753 Ohara, T., Akimoto, H., Kurokawa, J., Horii, N., Yamaji, K., Yan, X., and Hayasaka, T.: An Asian emission
754 inventory of anthropogenic emission sources for the period 1980–2020, Atmos. Chem. Phys., 7, 4419–4444,
755 doi:10.5194/acp-7-4419-2007, 2007.

Ojha, N., Naja, M., Singh, K. P., Sarangi, T., Kumar, R., Lal, S., Lawrence, M. G., Butler, T. M., and Chandola, H. C.: Variabilities in ozone at a semi-urban site in the Indo-Gangetic Plain region: Association with the meteorology and regional process, J. Geophys. Res., 117, D20301, doi:10.1029/2012JD017716, 2012.

Ojha, N., Naja, M., Sarangi, T., Kumar, R., Bhardwaj, P., Lal, S., Venkataramani, S., Sagar, R., Kumar, A., and Chandola, H. C.: On the processes influencing the vertical distribution of ozone over the central Himalayas: Analysis of yearlong ozonesonde observations, Atmos. Environ., 88, 201–211, doi:10.1016/j.atmosenv.2014.01.031, 2014.

Ojha, N., Pozzer, A., Rauthe-Schöch, A., Baker, A. K., Yoon, J., Brenninkmeijer, C. A. M., and Lelieveld, J.: Ozone and carbon monoxide over India during the summer monsoon: regional emissions and transport, Atmos. Chem. Phys., 16, 3013-3032, doi:10.5194/acp-16-3013-2016, 2016.

Otte, T. L.: The impact of nudging in the meteorological model for retrospective air quality simulations. Part I: Evaluation against national observation networks, J. Appl. Meteor. Climatol., 47, 1853–1867, 2008.

Pozzer, A., Zimmermann, P., Doering, U. M., van Aardenne, J., Tost, H., Dentener, F., Janssens-Maenhout, G., and Lelieveld, J.: Effects of business-as-usual anthropogenic emissions on air quality, Atmos. Chem. Phys., 12, 6915-6937, doi:10.5194/acp-12-6915-2012, 2012.

Purkait, N. N., De, S., Sen, S., and Chakrabarty, D. K.: Surface ozone and its precursors at its two sites in the northeast coast of India, Indian Journal of Radio and Space Physics, 38, 86–97, 2009.

Reddy, B. S. K., Kumar, K. R., Balakrishnaiah, G., Gopal, K. R., Reddy, R. R., Ahammed, Y. N., Narasimhulu, K., Reddy, L. S. S., and Lal, S.: Observational studies on the variations in surface ozone concentration at Anantapur in southern India, Atmos. Res. 98, 125–139, 2010.

Renuka, K., Gadhavi, H., Jayaraman, A., Lal, S., Naja, M., and Rao, S.: Study of Ozone and NO2 over Gadanki – a rural site in South India, J. Atmos. Chem., 71, 95–112, doi:10.1007/s10874-014-9284-y, 2014.

Sarangi, T., Naja, M., Ojha, N., Kumar, R., Lal, S., Venkataramani, S., Kumar, A., Sagar, R., and Chandola, H. C.: First simultaneous measurements of ozone, CO and NOy at a high altitude regional representative site in the central Himalayas, J. Geophys. Res.-Atmos., 119, 1592–1611, doi:10.1002/2013JD020631, 2014.

Sarkar, S., Srivastava, R. K., and Sagar, K.: Diurnal Monitoring Of Surface Ozone And PM2.5 Concentration And Its Correlation With Temperature, INTERNATIONAL JOURNAL OF TECHNOLOGY ENHANCEMENTS AND EMERGING ENGINEERING RESEARCH, VOL 3, ISSUE 09, ISSN 2347-4289, 2015.

Schell, B., Ackermann, I. J., Hass, H., Binkowski, F. S., and Ebel, A.: Modeling the formation of secondary organic aerosol within a comprehensive air quality model system, J. Geophys. 20 Res.-Atmos., 106, 28275–28293, doi:10.1029/2001JD000384, 2001.

Sillman, S.: The use of NOy, H2O2 and HNO3 as indicators for ozone-NOx-hydrocarbon sensitivity in urban locations, J. Geophys. Res., 100, 14175–14188, 1995.

789 Sinha, V., Kumar, V., and Sarkar, C.: Chemical composition of pre-monsoon air in the Indo-Gangetic Plain
790 measured using a new PTR-MS and air quality facility: high surface ozone and strong influence of biomass
791 burning, Atmos. Chem. Phys., 14, 5921-5941, 2014.

792 Stauffer, D. R., and Seaman, N. L.: Use of four-dimensional data assimilation in a limited area mesoscale model.
793 Part I: Experiments with synoptic-scale data, Monthly Weather Review 118, 1250- 1277, 1990.

794 Stauffer, D. R., Seaman, N. L. and Binkowski, F. S.: Use of four-dimensional data assimilation in a limited-area
795 mesoscale model. Part II: Effects of data assimilation within the planetary boundary layer, Monthly Weather
796 Review 119, 734-754, 1991.

797 Stockwell, W. R., Middleton, P., Chang, J. S., and Tang, X.: The second generation regional Acid Deposition
798 Model chemical mechanism for regional air quality modeling, J. Geophys. Res., 95, 16343-16367, 1990.

799 Taylor, K. E.: Summarizing multiple aspects of model performance in a single diagram, J. Geophys. Res. 106:
800 7183–7192, 2001.

801 Tewari, M., Chen, F., Wang, W., Dudhia, J., Lemone, M. A., Mitchell, K. E., Ek, M., Gayno, G., Wegiel, J. W.
802 and Cuenca, R.: Implementation and verification of the unified Noah land-surface model in the WRF model, 20th
803 Conference on Weather Analysis and Forecasting/16th Conference on Numerical Weather Prediction, Seattle,
804 WA, American Meteorological Society, 2004.

805 Wiedinmyer, C., Akagi, S. K., Yokelson, R. J., Emmons, L. K., Al-Saadi, J. A., Orlando, J. J., and Soja, A. J.: The
806 Fire INventory from NCAR (FINN): a high resolution global model to estimate the emissions from open burning,
807 Geosci. Model Dev., 4, 625–641, doi:10.5194/gmd-4-625-2011, 2011.

808 Wild, O., Zhu, X. and Prather, M. J.: Fast-J: Accurate simulation of in- and below cloud photolysis in tropospheric
809 chemical models, Journal of Atmospheric Chemistry, 37, 245-282, 2000.

810 Wilkinson, S., Mills, G., Illidge, R., and Davies,W. J.: How is ozone pollution reducing our food supply?, J. Exp.
811 Bot., 63, 527–536, doi:10.1093/jxb/err317, 2012.

812 Yadav, R., Sahu, L. K., Jaaffrey, S. N. A., and Beig, G.: Distributions of ozone and related trace gases at an urban
813 site in western India. J. Atmos. Chem. 71, 125–144, 2014.

814 Yoon, J. and Pozzer, A.: Model-simulated trend of surface carbon monoxide for the 2001–2010 decade, Atmos.
815 Chem. Phys., 14, 10465-10482, doi:10.5194/acp-14-10465-2014, 2014.

816 Zanis, P., Hadjinicolaou, P., Pozzer, A., Tyrlis, E., Dafka, S., Mihalopoulos, N., and Lelieveld, J.: Summertime
817 free-tropospheric ozone pool over the eastern Mediterranean/Middle East, Atmos. Chem. Phys., 14, 115-132,
818 doi:10.5194/acp-14-115-2014, 2014.

819 Zhang, Q., Streets, D. G., Carmichael, G. R., He, K. B., Huo, H., Kannari, A., Klimont, Z., Park, I. S., Reddy, S.,
820 Fu, J. S., Chen, D., Duan, L., Lei, Y., Wang, L. T., and Yao, Z. L.: Asian emissions in 2006 for the NASA
821 INTEX-B mission, Atmos. Chem. Phys., 9, 5131–5153, doi:10.5194/acp-9-5131-2009, 2009.

822 **Table 1.** Abbreviations/ Acronym

EDGAR	Emission Database for Global Atmospheric Research
HTAP	Hemispheric Transport of Air Pollution
IGP	Indo Gangetic plain
IST	Indian standard time
INTEX-B	Intercontinental Chemical Transport Experiment Phase B
MB	Mean Bias
MOZART	Model for Ozone and Related Chemical Tracers
NMB	Normalized mean bias
PBL	Planetary boundary layer
RMSD	Centered root mean squared difference
RRTM	Rapid Radiative Transfer Model
SEAC4RS	Southeast Asia Composition, Cloud, Climate Coupling Regional Study
WRF-Chem	Weather research and forecasting model coupled with chemistry

823

824

825 **Table 2.** Sub-regional estimates of anthropogenic emissions (in million mol h^{-1}) in the three emission inventories
826 used.

Region	**HTAP**			**INTEX-B**			**SEAC4RS**		
	NO_x	NMVOC	CO	NO_x	NMVOC	CO	NO_x	NMVOC	CO
North	8.1	14.0	110.0	6.3	10.0	96.1	8.7	10.7	86.9
East	5.8	10.1	102.9	6.0	6.9	78.8	6.7	8.2	72.4
West	2.9	4.6	31.0	1.8	2.1	24.7	3.7	2.9	24.3
Central	4.6	4.2	44.6	2.0	2.9	34.7	4.9	3.1	26.2
South	5.4	5.8	37.2	2.7	4.1	46.2	3.5	3.4	28.3
Total	26.8	38.7	325.7	18.8	26.0	280.5	27.5	28.3	238

827

828

829 **Table 3. A** brief description of the different WRF-Chem simulations conducted.

Sr. No.	**Simulation name**	**Emission Inventory**	**Year of Emission Inventory**	**Spatial Resolution of Emission Inventory**	**Chemical Mechanism**
1	HTAP-RADM2	HTAP	2010	0.1^ox 0.1^o	RADM2
2	INTEX-RADM2	INTEX-B	2006	0.5^ox 0.5^o	RADM2
3	S4RS-RADM2	SEAC4RS	2012	0.1^ox 0.1^o	RADM2
4	HTAP-MOZ	HTAP	2010	0.1^ox 0.1^o	MOZART-4

830
831
832
833
834
835
836
837

838 **Table 4.** List of observation sites and data sources used. Site nomenclature in brackets in column 1 is used in
839 figures 1, 5, 6, 9 and 10.
840

Site	Type	Latitude	Longitude	Altitude (m.a.s.l)	Data period	Reference
Mohali (MOH)	Urban	30.7°N	76.7°N	310	May 2012	Sinha et al. (2014)
Nainital (NTL)	Highly complex	29.37°N	79.45°E	1958	Apr 2011	Sarangi et. al. (2014)
Pantnagar (PNT)	Urban/ complex	29.0°N	79.5°E	231	Apr 2009-11	Ojha et al. (2012)
Delhi (DEL)	Urban	28.65°N	77.27°E	220	Apr 2013	SAFAR data
Dibrugarh (DBG)	Rural/ complex	27.4°N	94.9°E	111	Apr 2010-13	Bhuyan et al. (2014)
Darjeeling*	Complex	27.01°N	88.25°E	2134	Apr 2004	Lal (2007)
Kanpur (KNP)	Urban	26.46°N	80.33°E	125	Mar-May 2010-13	Gaur et al. (2014)
Mt. Abu (ABU)	Highly complex	24.6°N	72.7°E	1680	Apr 1993-2000	Naja et al. (2003)
Udaipur (UDP)	Urban	24.58°N	73.68°E	598	Apr 2010	Yadav et al. (2014)
Jabalpur (JBL)	Complex	23.17°N	79.92°E	411	Apr 2013	Sarkar et al. (2015)
Ahmedabad (ABD)	Urban	23.03°N	72.58°E	53	May 2011	Mallik et al. (2015)
Haldia (HAL)	Urban/ coastal	22.05°N	88.03°E	8	Apr 2004	Purkait et al. (2009)
Bhubaneshwar (BBR)	Urban	21.25°N	85.25°E	45	Mar-May 2010	Mahapatra et al. (2012)
Joharapur (JHP)	Rural	19.3°N	75.2°E	474	Apr 2002-2004	Debaje et al. (2006)
Pune (PUN)	Urban	18.54°N	73.81°E	559	Mar-May 2013	SAFAR data
Anantapur (ANP)	Rural	14.62°N	77.65°E	331	Apr 2009	Reddy et al. (2010)
Gadanki (GDK)	Rural	13.48°N	79.18°E	375	Mar-May 2010-11	Renuka et al. (2014)
Kannur (KNR)	Rural/ coastal	11.9°N	75.4°E	5	Apr 2010	Nishanth et al. (2012)
Thumba/ Trivendrum (TRI)	Urban/ coastal	8.55°N	77°E	3	Apr 2009	David et al. (2011)

841
842 * At Darjeeling only monthly mean value is available.
843
844
845 **Table 5.** A comparison of correlation coefficients (r) over different regions for the four simulations

Region	HTAP-RADM2	INTEX-RADM2	S4RS-RADM2	HTAP-MOZ
North	0.90	0.86	0.88	0.90
East	0.98	0.97	0.97	0.98
West	0.99	0.98	0.98	0.99
Central	0.70	0.67	0.69	0.75
South	0.99	0.98	0.97	0.97
Overall	0.98	0.97	0.97	0.99

846
847
848

849 **Table 6.** A comparison of noontime (1130-1630 IST) average mean biases in ppbv over different regions for the
850 four simulations.

Region	HTAP-RADM2	INTEX-RADM2	S4RS-RADM2	HTAP-MOZ
North	2.4	-3.3	-4.1	8.3
East	19.5	19.5	15.3	29.9
West	11.4	8.0	9.0	14.0
Central	0.9	-8.0	-2.5	8.8
South	15.3	8.2	6.5	25.5
Overall	10.5	5.9	5.2	17.3

851
852
853
854
855 **Table 7.** Recommendations based on noontime average mean biases over different regions for the four
856 simulations.

Region	HTAP-RADM2	INTEX-RADM2	S4RS-RAMD2	HTAP-MOZ
North	√			
East			√	
West		√		
Central	√			
South			√	
Overall			√	

857
858
859
860
861
862
863
864
865
866

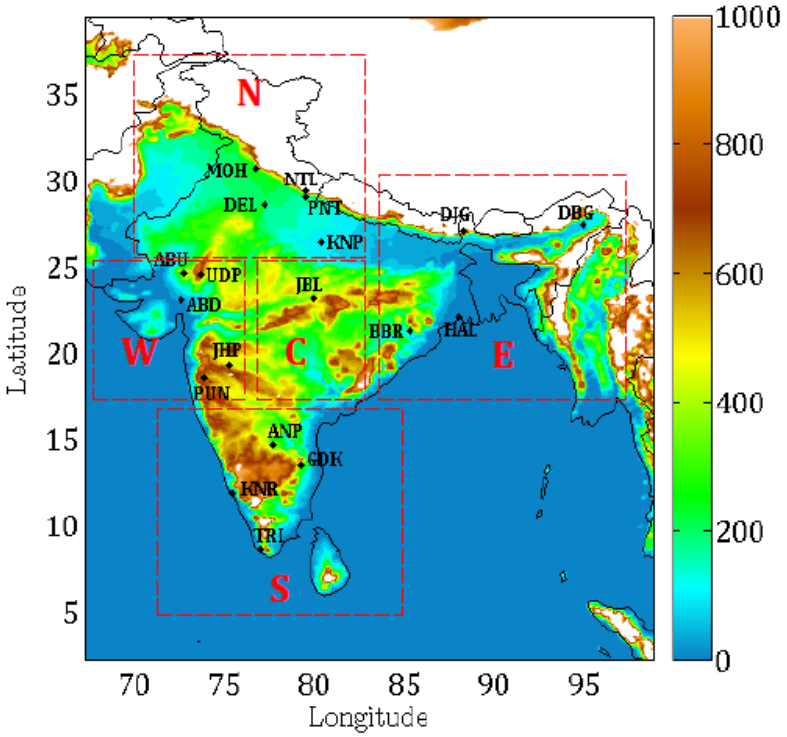

Figure 1. Simulation domain showing terrain height (in metres) and observation sites. White region indicates that the terrain height is equal to or exceeds 1 km. The domain is subdivided into five regions viz. North (N), South (S), East (E), West (W) and central (C) regions, as shown by red rectangles.

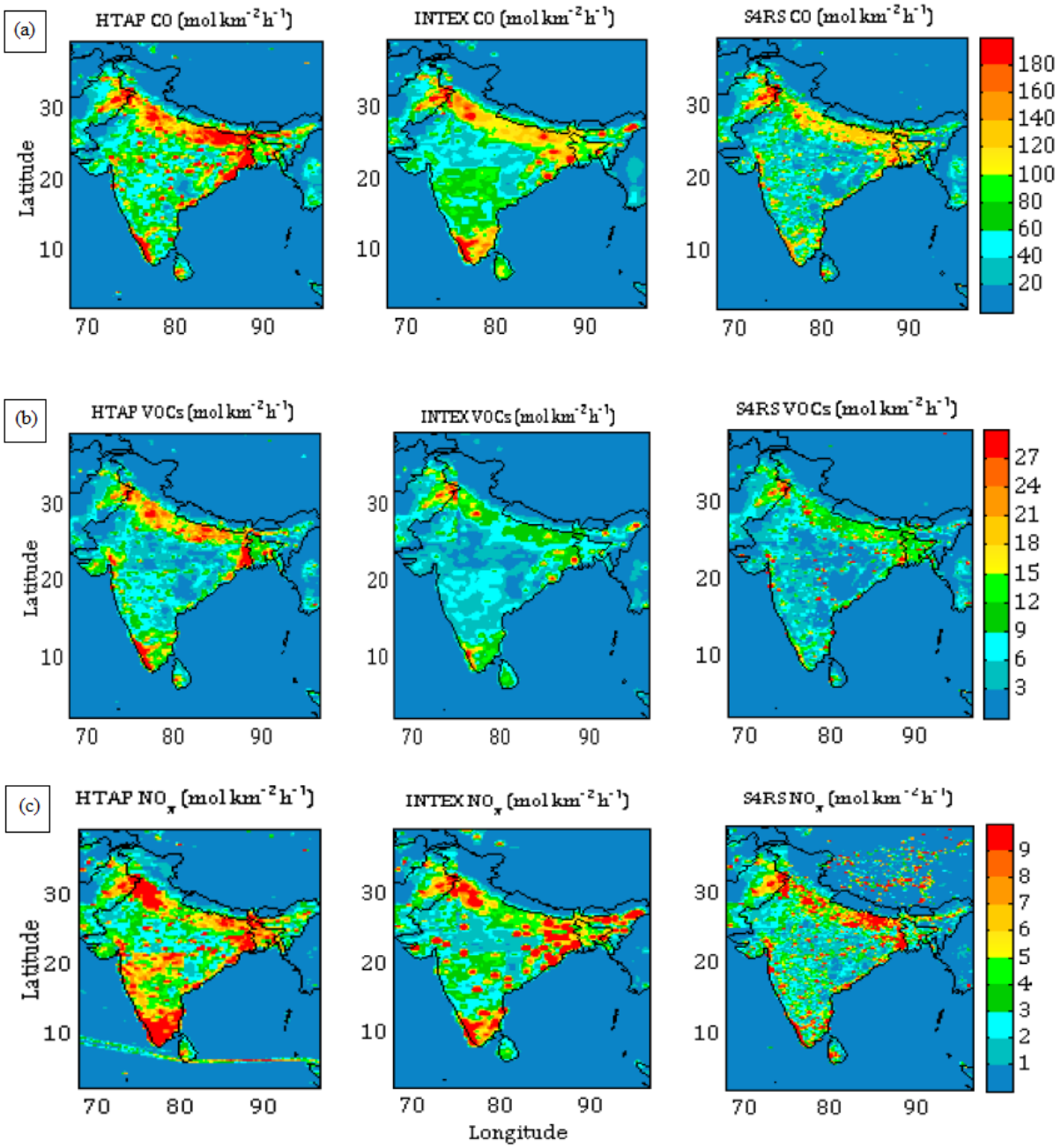

887

888 **Figure 2.** Comparison of (a) CO, (b) NMVOC and (c) NO_x emissions between the three inventories used (see Section-2.2 for
889 description).

890

891

892

893

894

895

896

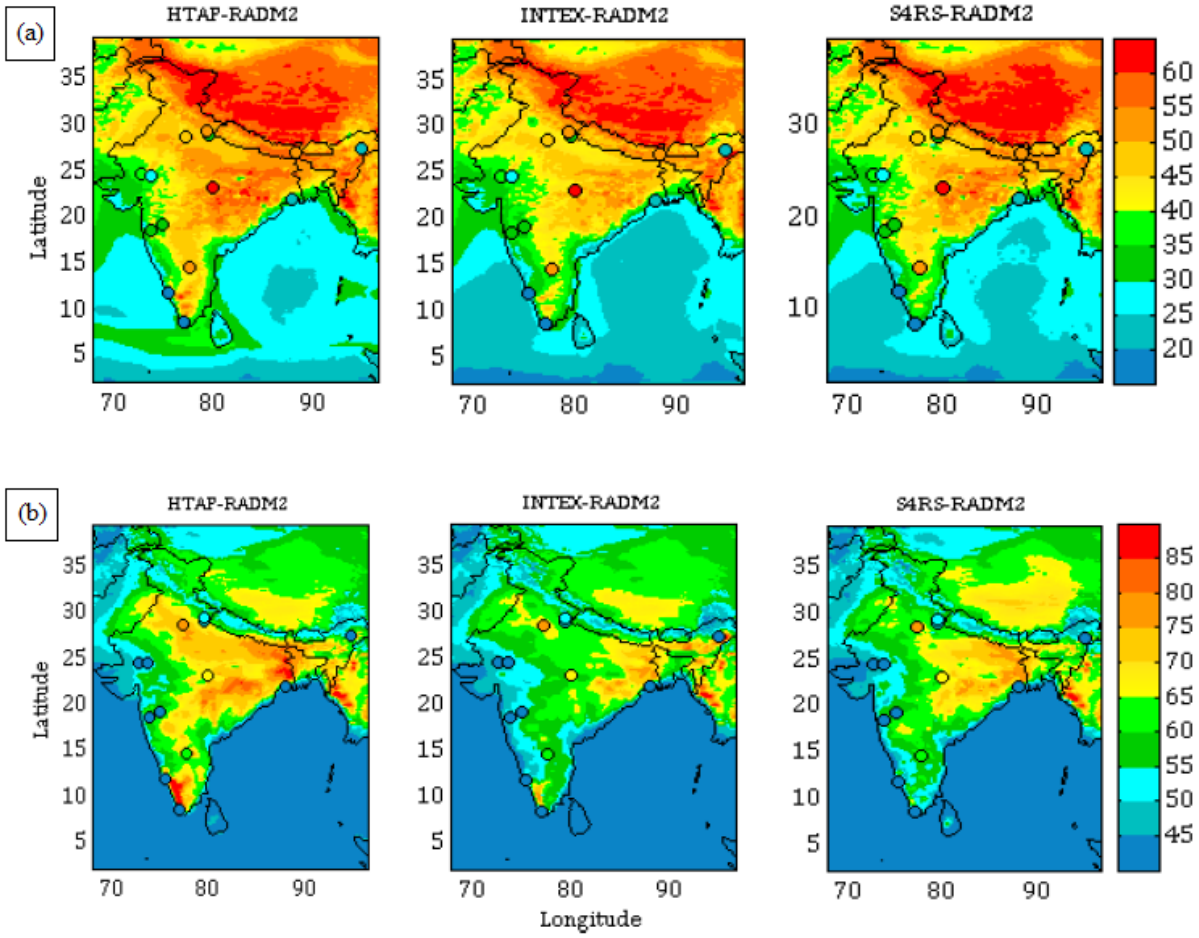

Figure 3. Monthly (April) average surface ozone calculated for (a) 24 h and (b) noontime (1130-1630 IST). The average ozone mixing ratios (ppbv) from observations are also shown for comparison on the same colour scale. Note the difference in colour scales in the top and bottom rows.

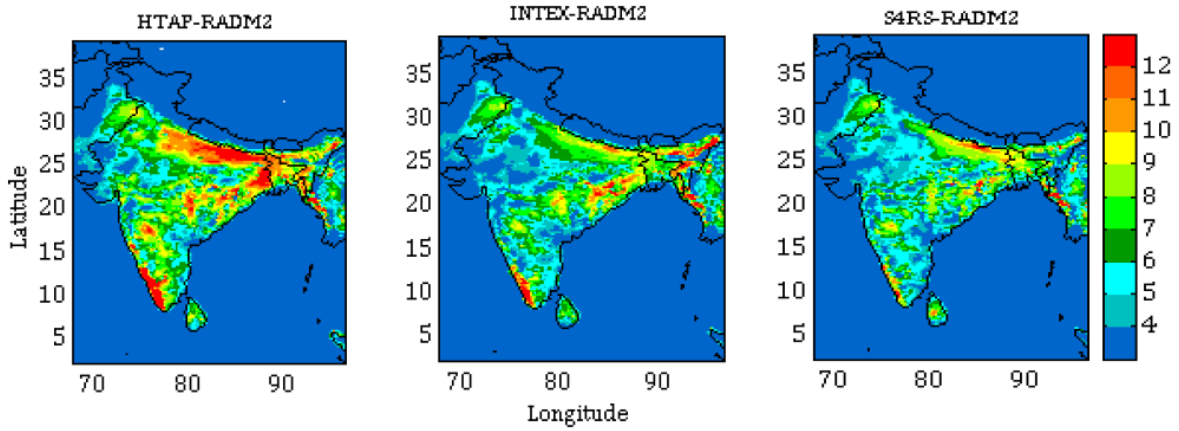

910
911 **Figure 4.** Net daytime surface ozone chemical tendency (in ppbv h^{-1}) for the month April during 0630-1230 IST.
912
913
914
915
916
917
918
919
920
921
922
923
924
925
926
927
928
929
930
931
932
933

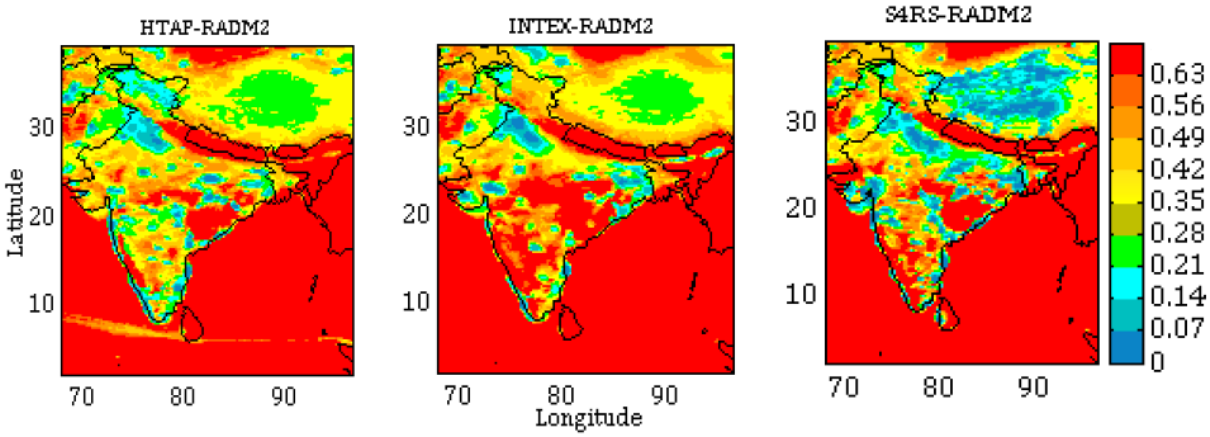

934

Figure 5. Net daytime surface CH_2O to NO_y ratio in simulations with different inventories for the month April during 0630-1230 IST.

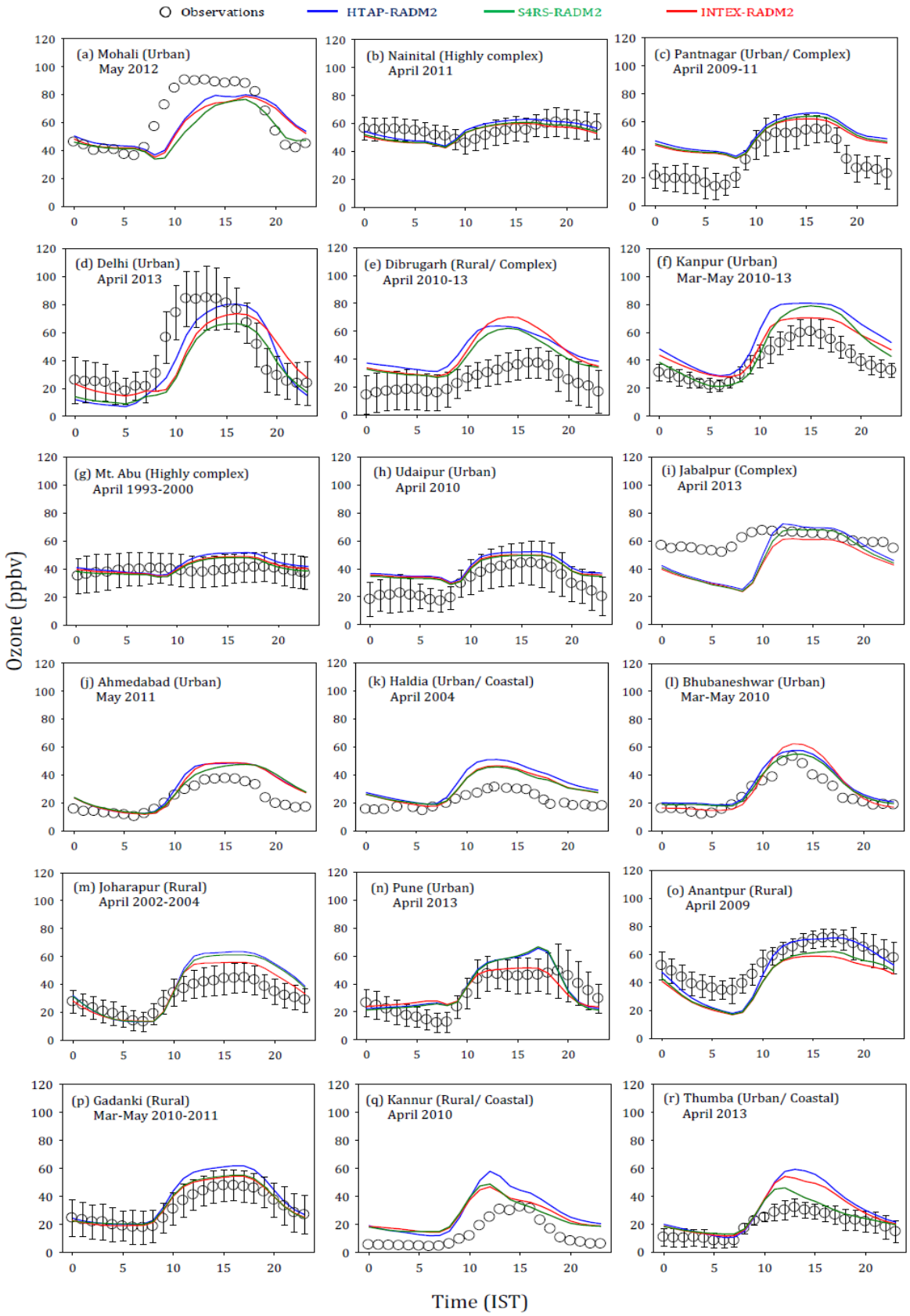

Figure 6. Comparison of monthly average diurnal variation of surface ozone simulated using different emission inventories at various observation sites. The observational data is available for the period indicated in the figure whereas all model simulations are for the year 2013. Error bars represent the temporal standard deviations of the monthly averages. All model simulations are with RADM2 chemistry.

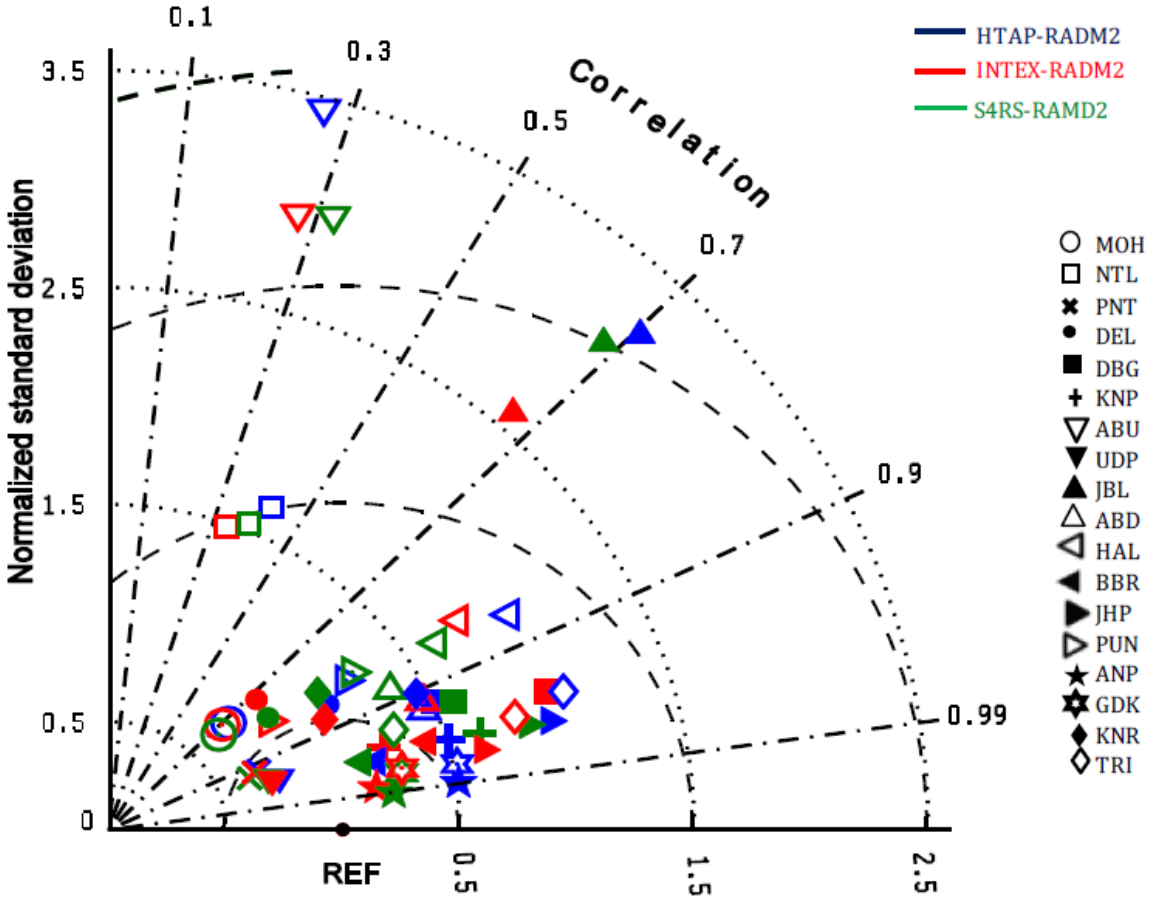

Figure 7. Taylor diagram with summary model statistics (r, normalized standard deviation and RMSD) at all sites. The correlation is the cosine of the angle from the horizontal axis, the root mean square difference is the distance from the reference point (REF) and the standard deviation is the distance from the origin.

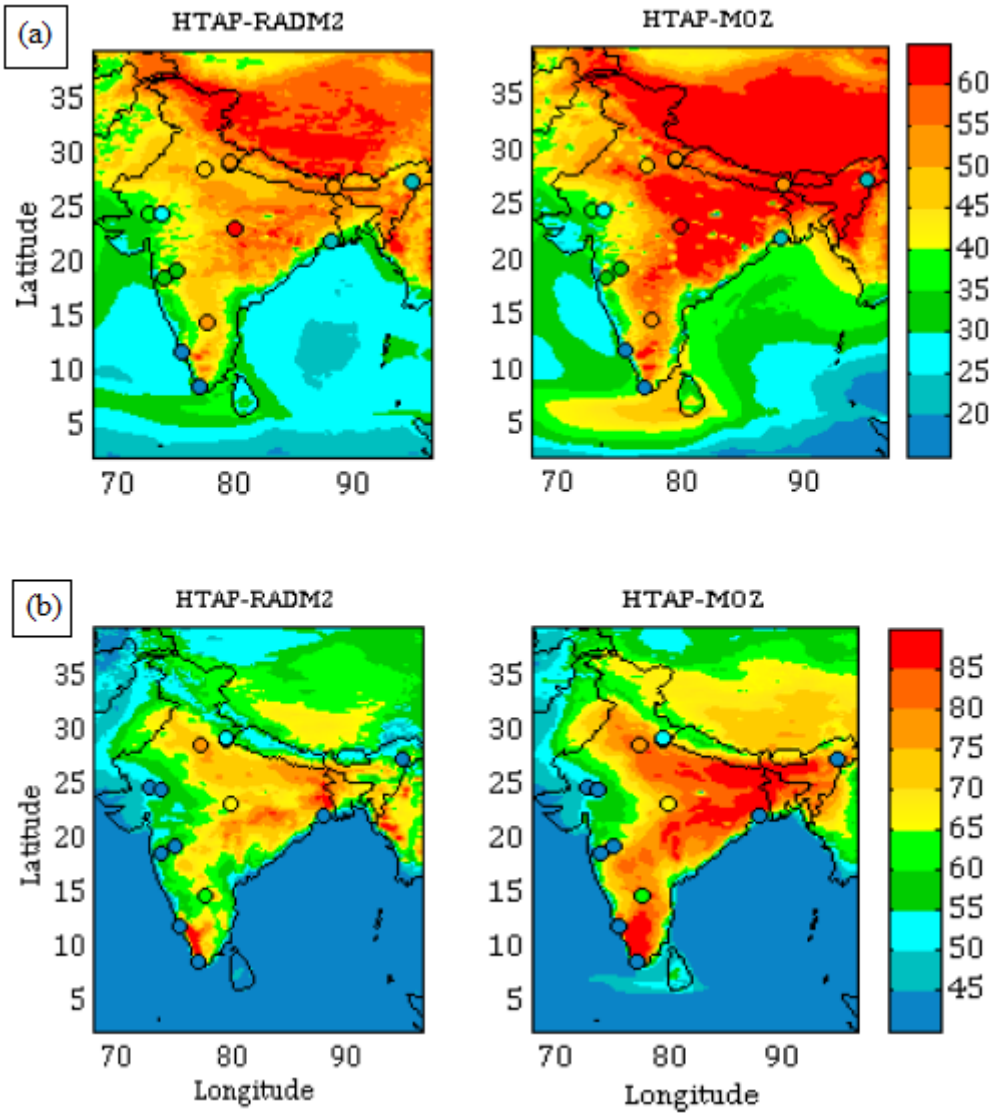

Figure 8. Monthly (April) average surface ozone calculated for (a) 24 h and (b) noontime (1130-1630 IST), comparing the chemical mechanisms (RADM2 and MOZART). The average ozone mixing ratios (ppbv) from observations are also shown for comparison on the same colour scale. Note the difference in colour scales in the top and bottom rows.

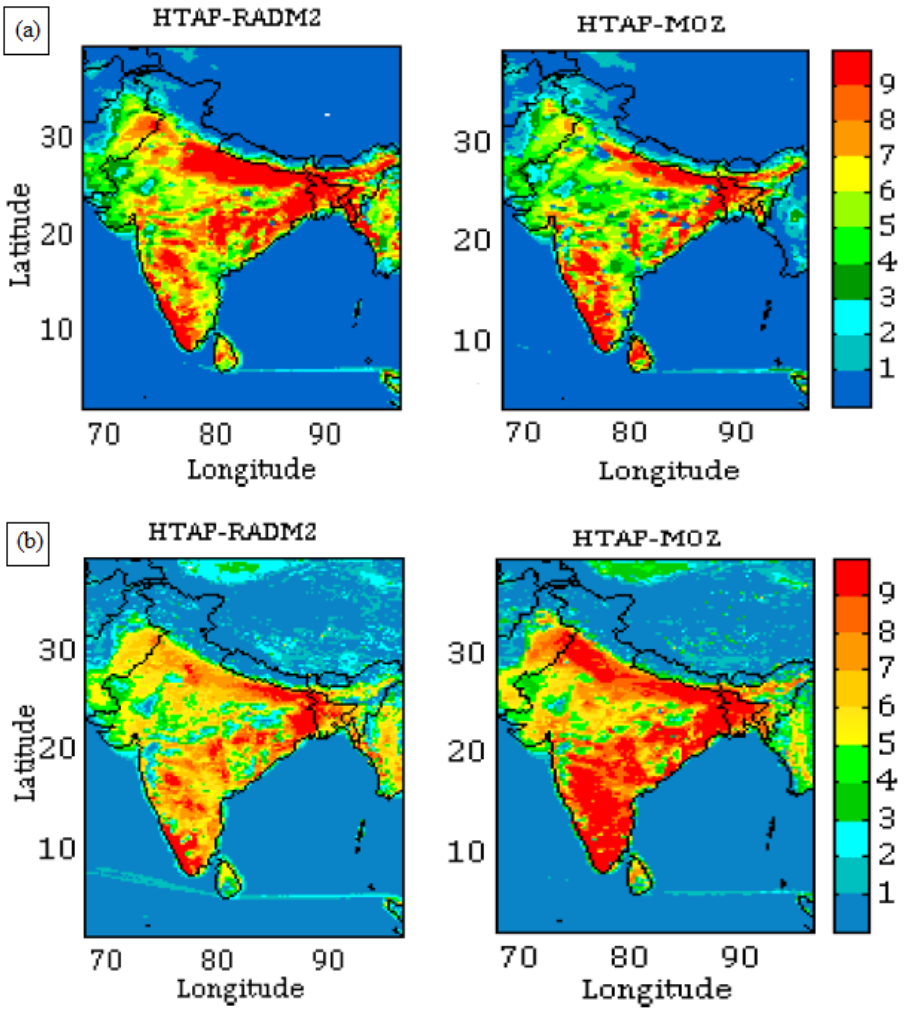

Figure 9. Average **(a)** net daytime surface ozone chemical tendency (in ppbv h^{-1}) **(b)** net daytime surface ozone chemical +vertical mixing tendency (in ppbv h^{-1}) for April during 0630-1230 IST

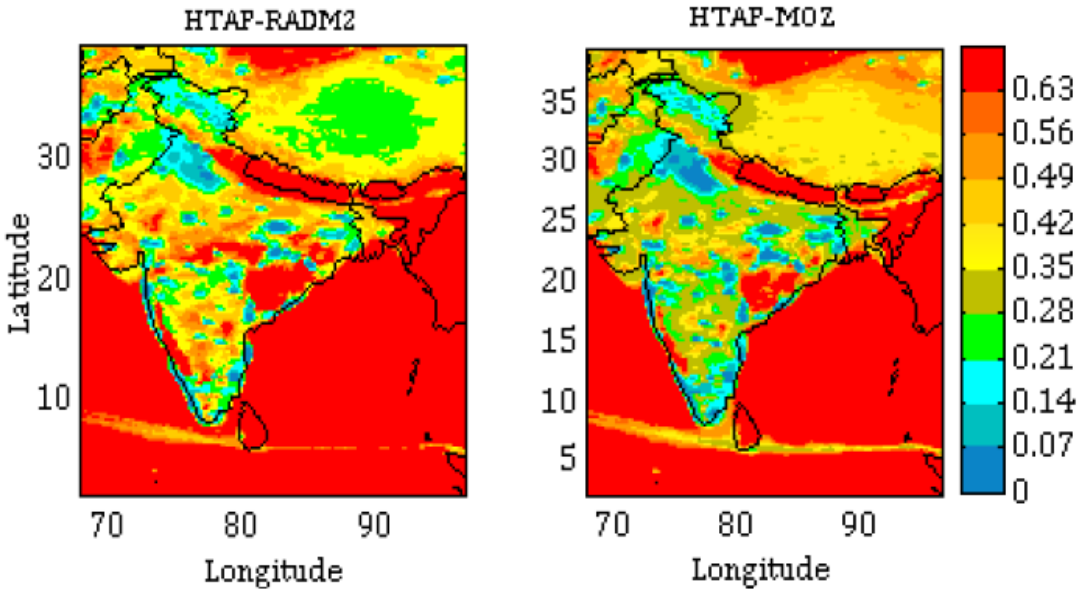

992
993 **Figure 10.** Net daytime surface CH_2O to NO_y ratio in simulations with different chemical mechanisms for the month April
994 during 0630-1230 IST.
995

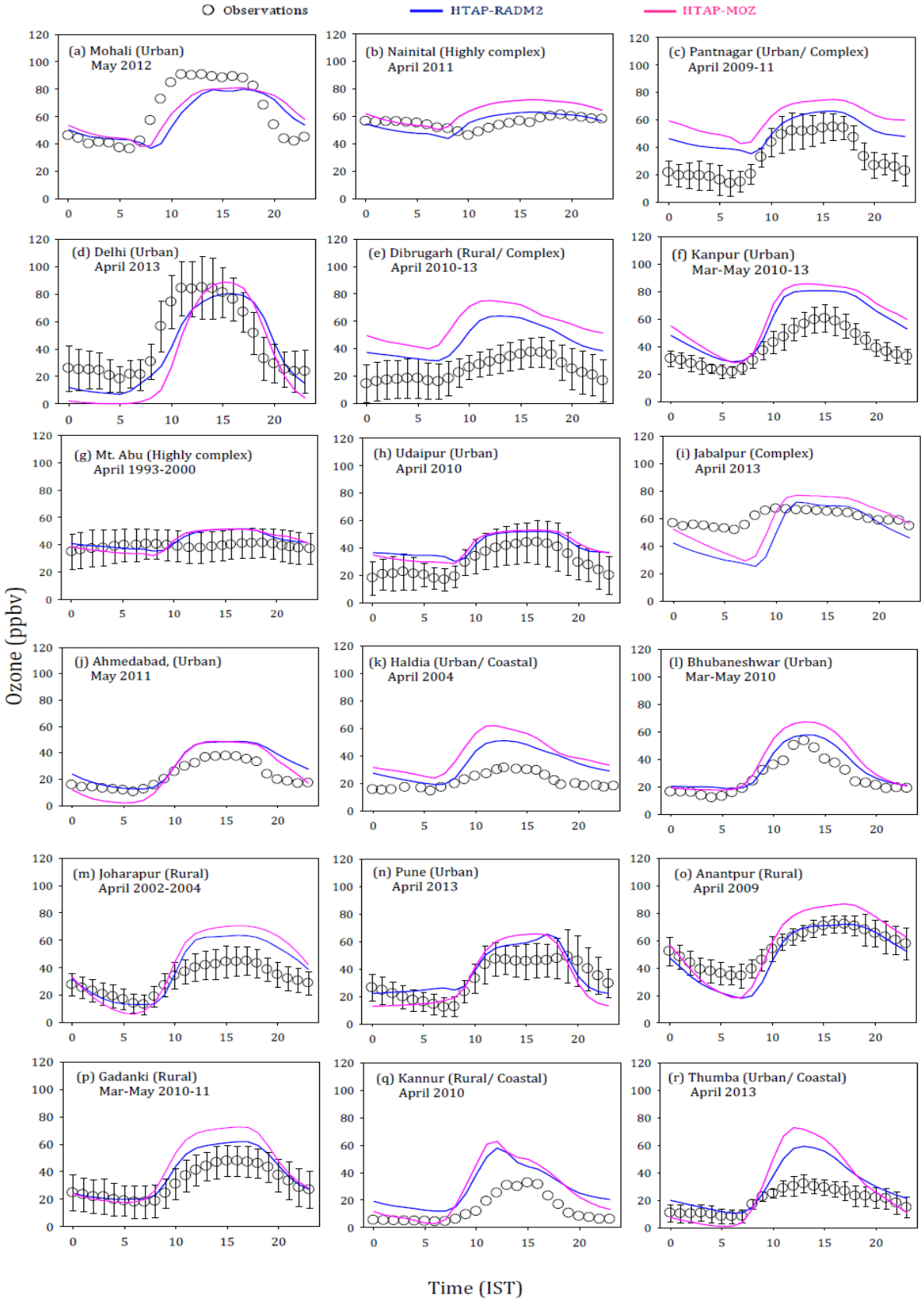

Figure 11. Comparison of monthly average diurnal variation of surface ozone simulated using different chemical mechanisms at various observation sites. The observational data is available for the period indicated in the figure whereas all the model simulations are for the year 2013. Error bars represent the temporal standard deviations of the monthly averages. All model simulations are with the HTAP inventory.

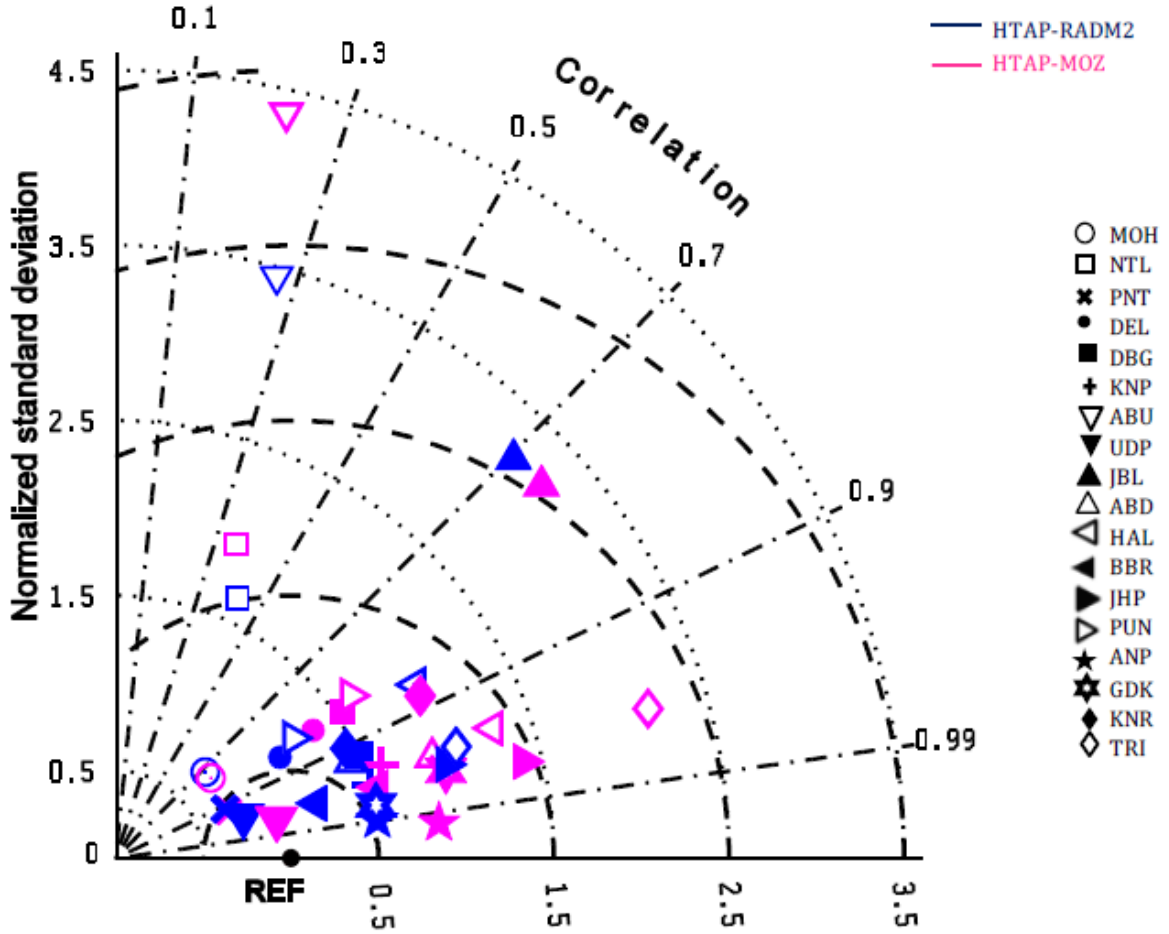

Figure 12. Taylor diagram with summary model statistics (r, normalized standard deviation and RMSD) at all sites. The correlation is the cosine of the angle from the horizontal axis, the root mean square difference is the distance from the reference point (REF) and the standard deviation is the distance from the origin.

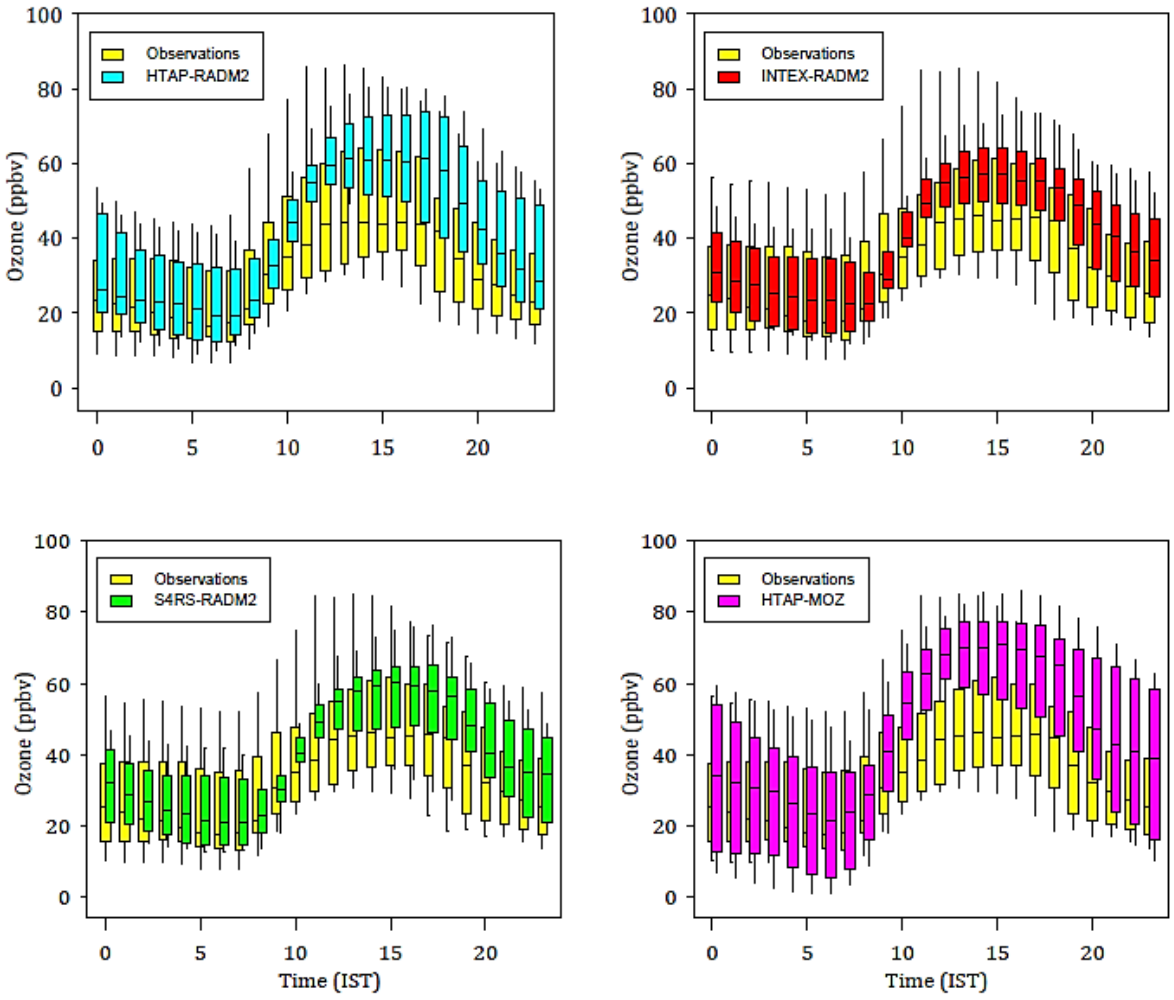

Figure 13. Box/whisker plot comparison of monthly average diurnal variation of surface ozone from model runs and observations over the entire domain (after spatially averaging the results). Upper and lower boundaries of boxes denote the 75th and 25th percentiles and whiskers represent the 95th and 5th percentiles. The line in the box is the median.

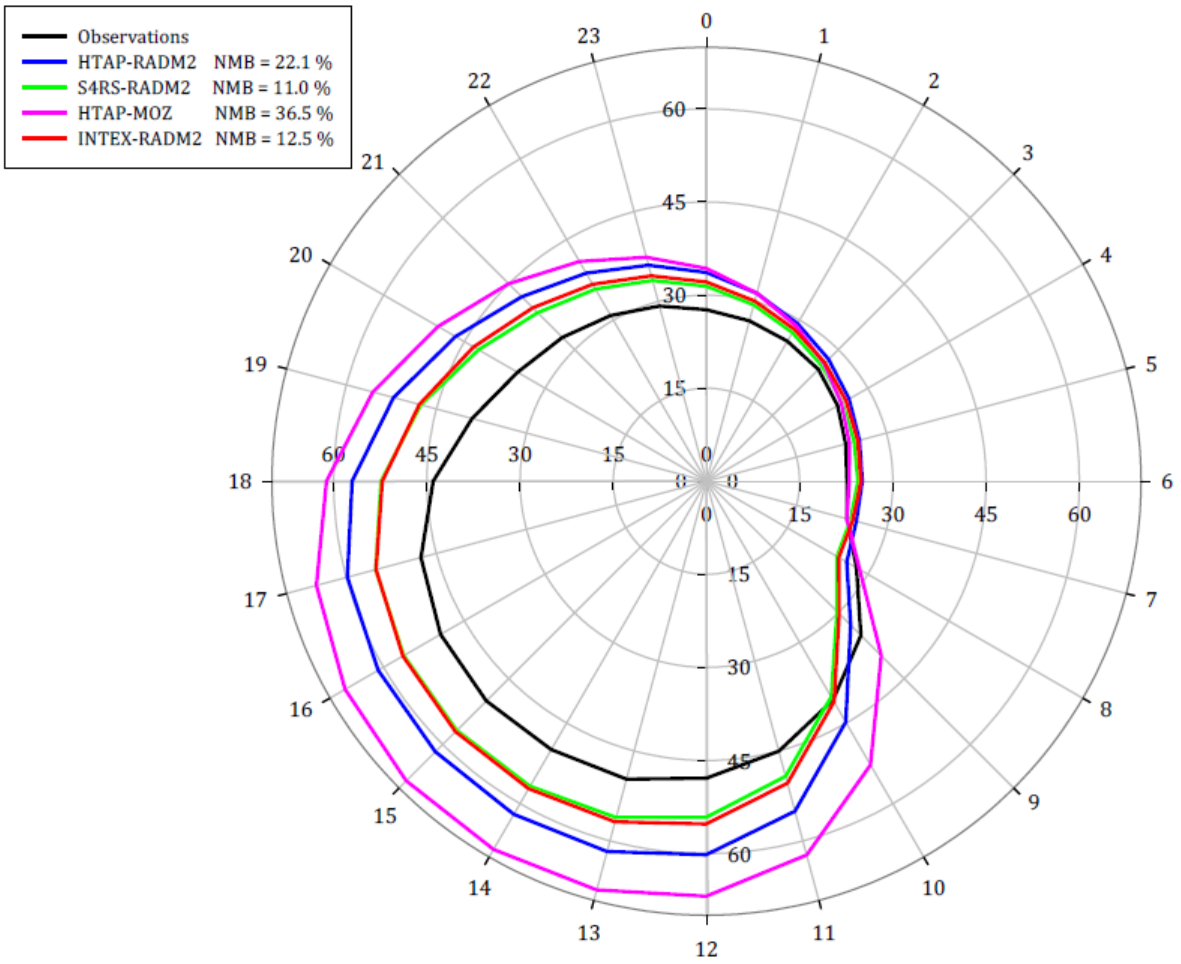

Figure 14. Polar plot for monthly mean diurnal variation of surface ozone (in ppbv) from all model simulations and observations each spatially averaged over all sites. The numbers on the outermost circle represent the hour of the day and the radial distance from the centre represents surface ozone mixing ratios in ppbv. The normalized mean biases (NMB in %) are indicated in the caption box.